Inter-organ Wingless/Ror/Akt signaling regulates nutrient-dependent hyperarborization of somatosensory neurons

AUTHOR(S):

Kanaoka, Yasutetsu; Onodera, Koun; Watanabe, Kaori; Hayashi, Yusaku; Usui, Tadao; Uemura, Tadashi; Hattori, Yukako

CITATION:

Kanaoka, Yasutetsu ...[et al]. Inter-organ Wingless/Ror/Akt signaling regulates nutrient-dependent hyperarborization of somatosensory neurons. eLife 2023, 12: e79461.

ISSUE DATE:

2023

URL:

http://hdl.handle.net/2433/278855

eLife
RESEARCH ARTICLE

Inter-organ Wingless/Ror/Akt signaling regulates nutrient-dependent hyperarborization of somatosensory neurons

Yasutetsu Kanaoka[1], Koun Onodera[1], Kaori Watanabe[1], Yusaku Hayashi[1], Tadao Usui[1], Tadashi Uemura[1,2,3]*, Yukako Hattori[1,4]*

[1]Graduate School of Biostudies, Kyoto University, Kyoto, Japan; [2]Research Center for Dynamic Living Systems, Kyoto University, Kyoto, Japan; [3]AMED-CREST, Tokyo, Japan; [4]JST FOREST, Tokyo, Japan

Abstract Nutrition in early life has profound effects on an organism, altering processes such as organogenesis. However, little is known about how specific nutrients affect neuronal development. Dendrites of class IV dendritic arborization neurons in *Drosophila* larvae become more complex when the larvae are reared on a low-yeast diet compared to a high-yeast diet. Our systematic search for key nutrients revealed that the neurons increase their dendritic terminal densities in response to a combined deficiency in vitamins, metal ions, and cholesterol. The deficiency of these nutrients upregulates Wingless in a closely located tissue, body wall muscle. Muscle-derived Wingless activates Akt in the neurons through the receptor tyrosine kinase Ror, which promotes the dendrite branching. In larval muscles, the expression of *wingless* is regulated not only in this key nutrient-dependent manner, but also by the JAK/STAT signaling pathway. Additionally, the low-yeast diet blunts neuronal light responsiveness and light avoidance behavior, which may help larvae optimize their survival strategies under low-nutritional conditions. Together, our studies illustrate how the availability of specific nutrients affects neuronal development through inter-organ signaling.

Editor's evaluation

Nutrition profoundly affects neural development. The Uemura lab previously reported that C4da neurons elaborate complex dendrites when larvae grow on low-yeast diets, a phenomenon called neural sparing. In the current study, they define the molecular mechanism underlying the nutrition-mediated phenomenon and identify that the inter-organ Wingless/Ror/Akt pathway between the neuron and its adjacent muscles is necessary and sufficient to mediate dendrite over-branching in the low-yeast condition.

***For correspondence:** tauemura@lif.kyoto-u.ac.jp (TU); yhattori@lif.kyoto-u.ac.jp (YH)

Competing interest: The authors declare that no competing interests exist.

Funding: See page 20

Preprinted: 01 May 2022
Received: 13 April 2022
Accepted: 11 December 2022
Published: 17 January 2023

Reviewing Editor: K VijayRaghavan, National Centre for Biological Sciences, Tata Institute of Fundamental Research, India

Introduction

The physiological state of an organism influences organogenesis throughout the body. Among many external factors affecting the physiological state, nutrition in early life has a profound impact (***Bhutta et al., 2017***). This is particularly the case with neural development, which is highly metabolically demanding. A large amount of energy is consumed to control neural stem cell division, form complex dendrites and long axons in myriad neuronal cell types, and ultimately construct functional neural circuits (***Prado and Dewey, 2014***; ***Georgieff et al., 2015***). Compared to metabolic regulation of neural stem cell proliferation (***Homem et al., 2015***), little is known about how nutritional status is

conveyed to developing neurons and how those neurons regulate growth in response to such a signal (***Shimada-Niwa and Niwa, 2014***; ***Shimono et al., 2014***; ***Liu et al., 2017***).

Dietary nutrients are absorbed by the digestive tract and circulated throughout the body, and they are sensed by organs including the nervous system (***Chantranupong et al., 2015***). Those organs communicate the nutritional status to each other by secreting signaling molecules, either low-molecular-weight metabolites or macromolecules such as soluble proteins and lipoprotein particles, to elicit tissue-specific responses; and it is this inter-organ communication network that coordinates organogenesis with body growth (***Droujinine and Perrimon, 2016***; ***Texada et al., 2020***). In the nervous system, neurons sense circulating nutrients directly or by way of signaling molecules derived from other tissues, so there exist diverse modes of nutrient sensing (***Morton et al., 2014***; ***Jayakumar and Hasan, 2018***).

The above-mentioned regulatory mechanisms of nutrient-dependent neuronal development can be explored at the molecular level with appropriate model neurons; and one particularly amenable model is the *Drosophila* class IV dendritic arborization (C4da) neuron located in the larval periphery (***Grueber et al., 2002***). Dendritic arbors of C4da neurons extensively cover the body wall, and they are elaborated two-dimensionally between the epidermis and the body wall muscles. C4da neurons in larvae respond to noxious thermal, mechanical, and light stimuli and provoke robust avoidance behaviors (***Tracey et al., 2003***; ***Hwang et al., 2007***; ***Xiang et al., 2010***; ***Zhong et al., 2010***; ***Guntur et al., 2015***; ***Chin and Tracey, 2017***). In the context of adaptation of growing animals to nutritional environments, it has been shown more recently that the C4da neurons sense amino acid deprivation by an amino acid transporter, Slimfast, at a late larval stage, which contributes to overcoming the nutritional stress, thereby allowing pupariation (***Jayakumar et al., 2016***; ***Jayakumar et al., 2018***). In addition, we and another group have shown that dendrites of C4da neurons become more complex when larvae are reared on low-yeast diets compared to high-yeast diets (***Figure 1A and B***, and ***Figure 1—figure supplement 1A***; ***Watanabe et al., 2017***; ***Poe et al., 2020***). We designate this counterintuitive phenotype as hyperarborization. Although the entire larval development takes longer on the low-yeast diet compared to the high-yeast diet (***Figure 1—figure supplement 1A***), it is unlikely that the hyperarborization is a simple consequence of the longer larval stage (***Watanabe et al., 2017***; see also Results). Therefore, it has been assumed that the low-yeast diet is deficient in select nutrients, which causes the phenotype. However, the identities of such key nutrients responsible for the hyperarborization phenotype have heretofore not been determined.

A wealth of genetic analyses on standard foods has revealed numerous regulators of dendrite morphogenesis working either in cell-autonomous or non-cell autonomous manners (***Jan and Jan, 2010***; ***Dong et al., 2015***; ***Valnegri et al., 2015***). Some of the cell-autonomous mechanisms include those related to intake and synthesis of metabolites: amino acid transporter SLC36/Pathetic (Path) (***Lin et al., 2015***) and a critical regulator of fatty acid synthesis, sterol regulatory element binding protein (SREBP) (***Meltzer et al., 2017***; ***Ziegler et al., 2017***). Concerning the non-cell autonomous mechanisms, direct interactions between C4da neurons and one of the adjacent tissues, the epidermis, have been well characterized with the help of anatomical approaches under both light and electron microscopes (***Yang and Chien, 2019***). Some portions of dendritic branches are attached to the extracellular matrix, and the attachment is mediated by signaling between an epidermally derived semaphorin ligand Sema-2b and its receptor Plexin B (PlexB) on the dendrite (***Meltzer et al., 2016***), as well as between a TGF-β ligand Maverick (Mav)-Ret receptor combination (***Hoyer et al., 2018***). Other portions of dendritic arbors are wrapped by epidermal cells, so overall the dendrite arbor is embedded in the epidermis locally (***Han et al., 2012***; ***Kim et al., 2012***; ***Tenenbaum et al., 2017***; ***Jiang et al., 2019***). In contrast to the above dendrite-epidermis interaction, there is much less evidence for signaling between muscles and dendrites, despite their proximity to dendrites and their large volume in the body (***Yasunaga et al., 2010***). Furthermore, when considering the relationship between nutritional status and C4da neurons, little is known about how exactly the dietary information is remotely transmitted from the gut to the neurons. To address these unsolved questions, it is critical to efficiently quantify the effects of various nutritional and genetic conditions on this nutrition-dependent hyperarborization. For this purpose, we developed DeTerm, a software program for automatic detection of dendritic branch terminals (***Figure 1A and B***; ***Kanaoka et al., 2019***).

Here, we show that C4da neurons increase their dendritic terminal density on a low-yeast diet (LYD) compared to a high-yeast diet (HYD) due to a concurrent deficiency in vitamins, metal ions, and

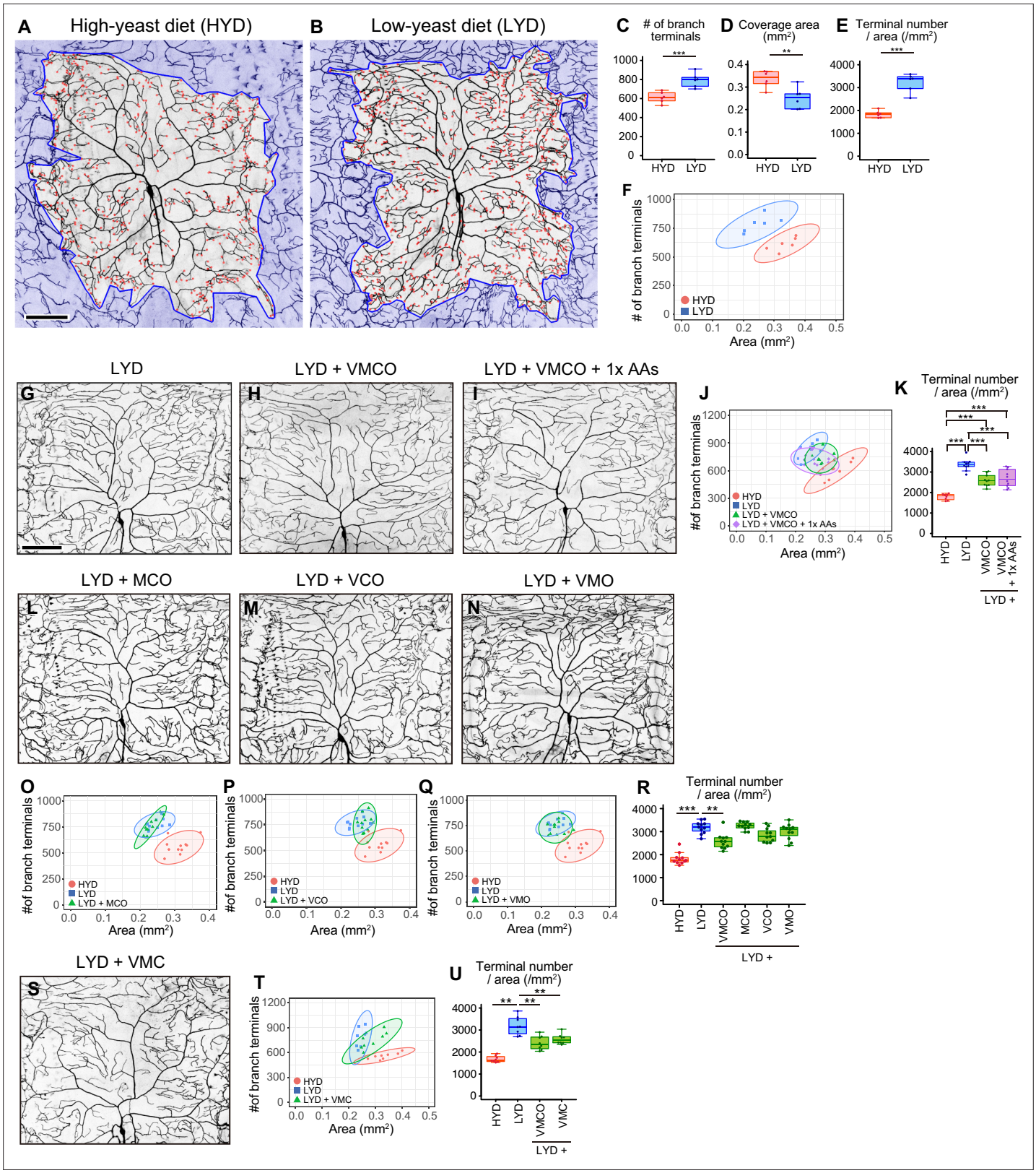

Figure 1. A mixture of vitamins, metal ions, and cholesterol ameliorates C4da neuron hyperarborization. (**A and B**) Representative output images of DeTerm. DeTerm automatically detects dendritic terminals of C4da neuron ddaC in larvae reared on a high-yeast diet (HYD; **A**) or a low-yeast diet (LYD; **B**). Red points indicate detected branch terminals. (**C–E**) The numbers of branch terminals detected by DeTerm (**C**), coverage areas of dendrites (**D**), and densities of branch terminals (the number of branch terminals/coverage area; **E**) of individual neurons, on HYD or LYD (Student's t-test, n=6). Boxes show

Figure 1 continued on next page

Figure 1 continued

the 25th–75th percentiles. The central lines indicate the medians. Whiskers extend to the most extreme data points, which are no more than 1.5 times the interquartile range. Boxes and points for HYD data and those for LYD data are colored red and blue, respectively, in this and subsequent figures. (**F**) Two-dimensional (2D) plot of the dendritic area and the number of branch terminals of each neuron. The ellipses represent the 95% confidence intervals, which are clearly separated for HYD and LYD. This plot shows a positive correlation between the area of the dendritic field and the number of branch terminals. (**G–I**) Images of ddaC neurons in larvae reared on LYD (**G**), LYD +vitamin + metal ion +cholesterol + other ingredients (LYD +VMCO; **H**), or LYD +VMCO + 1 x amino acids (LYD +VMCO + 1 x AAs; **I**). (**J and K**) Quantitative analysis of ddaC on LYD +VMCO or LYD +VMCO + 1 x AAs. (**J**) 2D plot. Note that the ellipse of LYD +VMCO and that of LYD +VMCO + 1 x AAs are located between those of HYD and LYD. (**K**) Densities of branch terminals (One-way ANOVA and Tukey's HSD test, n=8–10). (**L–N**) Images of ddaC neurons in larvae reared on LYD +metal ion+cholesterol + other ingredients (LYD +MCO; **L**), LYD +vitamin + cholesterol +other ingredients (LYD +VCO; **M**), or LYD +vitamin + metal ion +other ingredients (LYD +VMO; **N**). (**O–R**) 2D plots of ddaC on LYD +MCO (**O**), LYD +VCO (**P**), or LYD +VMO (**Q**), and densities of branch terminals (R, Steel test, n=10). The elipses of these diets largely overlap with that of LYD and clearly or almost separare from that of HYD (**O–Q**). (**S**) Images of ddaC neurons in larvae reared on LYD +vitamin + metal ion +cholesterol (LYD +VMC). (**T and U**) 2D plots of ddaC neurons in larvae reared on LYD +VMC (**T**) and densities of branch terminals (U, Steel test, n=8). The ellipse of LYD +VMC is located between those of HYD and LYD (**T**). Boxplots in (**K, R and U**) are depicted as in (**C**). *p<0.05, **p<0.01, and ***p<0.001. Scale bars, 100 μm.

The online version of this article includes the following figure supplement(s) for figure 1:

Figure supplement 1. Addition of amino acids does not rescue the hyperarborization.

Figure supplement 2. Extended larval growth is not associated with the hyperarborization.

cholesterol. We then identified an extrinsic factor and an intracellular signaling axis that jointly enable C4da neurons to respond to the LYD nutritional status. On LYD, Akt and its upstream receptor tyrosine kinase Ror in the neuron are required for the hyperarborization. In a paracrine fashion, Wingless (Wg) produced by body wall muscles activates Akt by way of Ror and contributes to the hyperarborization. In muscles of larvae on the HYD, Stat92E, a transcription factor in the JAK/STAT pathway, was more highly expressed and negatively regulated *wg* expression, whereas the LYD resulted in lower expression of *Stat92E*, which partly contributed to higher expression of *wg*. Together, our studies illustrate how nutritional environments impact neuronal development through the Wg-Ror-Akt pathway between the neuron and closely located muscles. As for the neuronal function, we found that LYD blunted light responsiveness of class IV neurons and larval light avoidance behavior, which may help larvae optimize their survival strategies under low-nutritional conditions.

Results

A mixture of vitamins, metal ions, and cholesterol ameliorates the hyperarborization

Our analysis using the software program called DeTerm established that both the number of branch terminals per neuron and the density of terminals (terminal number/arbor size) were higher on LYD than on HYD (***Figure 1C-E***). In addition to these box plots, we drew two-dimensional plots with the dendritic area on the X-axis and the number of branch terminals on the Y-axis, and the numerical features of dendrites of C4da neurons on HYD and those on LYD were clearly separated (***Figure 1F***). Therefore, in the subsequent analyses, we mainly focused on the density of branch terminals (***Figure 1E***) and the separation in 2D plots (***Figure 1F***) to evaluate the hyperarborization phenotypes.

Yeast is one of the main ingredients in *Drosophila* laboratory foods, and it has been primarily considered as a source of amino acids. We suspected the possibility that LYD is deficient in amino acids and that is the cause of the phenotype. Therefore, we first examined whether supplementation of LYD with amino acids would ameliorate the hyperarborization. However, the addition of an essential amino acid solution, an amino acid mix, or peptone resulted in only slight or no restoration of the phenotype (***Figure 1—figure supplement 1B–L***, and see details in the legend). To more comprehensively search for nutrients responsible for the hyperarborization, we used fractions of a fully chemically defined or holidic medium for *Drosophila* (***Piper et al., 2014***; ***Piper et al., 2017***) and examined which fraction or which combinations of the fractions were able to ameliorate the phenotype (***Figure 1—figure supplement 1A***). Addition of four fractions other than amino acids, which comprise vitamins (V), metal ions (M), cholesterol (C), and other ingredients (nucleic acids and lipid-related metabolites: O), to LYD significantly rescued the hyperarborization (***Figure 1G, H, J and K***; see also the legend of ***Figure 1J***). We named this diet LYD + VMCO. Further supplementation of amino acids to LYD + VMCO did not

improve the degree of the rescue (***Figure 1K***). Importantly, the phenotype was not restored without any one of three fractions, namely, vitamins, metal ions and cholesterol (***Figure 1L–R***). On the other hand, the fraction designated other ingredients was dispensable for amelioration of the phenotype (***Figure 1S-U***). These results suggest that the concurrent deficiency in vitamins, metal ions, and cholesterol contributes to the hyperarborization phenotype.

Larval developmental timing on LYD + VMC was comparable to that on LYD ***Figure 1—figure supplement 1A***; nonetheless the hyperarborization phenotype was blunted on LYD + VMC. We then examined whether extension of larval growth cause the hyperarborization by testing other dietary or genetic interventions. We previously compared dendrite morphologies between larvae reared on a low-sugar diet and those on a high-sugar diet that delays larval development (***Musselman et al., 2011***), and we reported that the hyperarborization does not occur on the high-sugar diet (***Watanabe et al., 2017***). We expanded this approach and analyzed the effect of the sugar overload on dendrite branching in a quantitative manner. When we observed dendrites in larvae reared on HYD supplemented with sucrose at the same timing as those on LYD (8–9 days AEL), they did not become more complex compared to those on HYD alone (***Figure 1—figure supplement 2A–E***). Moreover, we observed the C4da neurons in larvae with *dlip8* overexpressed in wing imaginal discs, which is sufficient to extend the larval stage (***Colombani et al., 2012***). This genetic intervention did not affect dendrite complexity (***Figure 1—figure supplement 2F–J***). Altogether, these results suggest that the prolonged larval period was not the primary cause of the hyperarborization phenotype.

Akt and receptor tyrosine kinase Ror are required in C4da neurons to hyperarborize their dendrites

To investigate the molecular mechanism underlying the hyperarborization phenotype on LYD, we focused on intracellular signaling factors that have been reported to sense nutritional status in other cellular contexts. Thus, we examined whether C4da neuron-specific knockdown (KD) of any of these factors would affect this diet-selective phenotype (***Figure 2A–J*** and ***Figure 2—figure supplement 1A–P***). To identify candidate genes whose KD attenuated the hyperarborization phenotype, we investigated how much the HYD ellipse and the LYD ellipse approached each other or overlapped in the 2D plot. We also compared the terminal density using two-way analysis of variance (ANOVA) throughout this study, unless described otherwise (see p-values in the aforementioned figures).

Among KD phenotypes of the candidate genes, we were interested in an *Akt kinase* (*Akt*) KD in one of the RNAi lines, which impacted hyperarborization but left overall dendritic architecture relatively intact (v2902; ***Figure 2B, E, G and H***). This *Akt* KD in the v2902 line resulted in neither apparent downsizing of the arbor area (***Figure 2G***) nor overt decreases in branch length on HYD (***Figure 2—figure supplement 2A and B***), contrasting with diet-independent severe phenotypes observed in another *Akt* RNAi line (BL33615; ***Figure 2C, F, I and J*** and ***Figure 2—figure supplement 2C and D***). Our subsequent analyses showed that v2902 was less effective in knocking down *Akt* than BL33615 (***Figure 2—figure supplement 3A–H***). We interpreted these results as follows: the severe reduction of Akt function in the BL33615 line impairs growth of dendritic branches, as shown previously (***Parrish et al., 2009***), whereas the mild reduction in the v2902 line mostly secures the basal activity of Akt necessary for growth, but it affects hyperarborization on LYD in a relatively selective manner (***Figure 2—figure supplement 2G–I***). We further knocked down genes that constitute the signaling pathways of Akt (***Figure 2—figure supplement 1Q-AJ***), and found that inhibition of TOR signaling components, such as *Target of rapamycin* (*Tor*) or *Ribosomal protein S6 kinase* (*S6k*) also ameliorated the phenotype (***Figure 2—figure supplement 1Q–AJ***). A similar effect caused by inhibition of *Tor* was described by ***Poe et al., 2020***.

Various secreted factors are known to function as inter-organ communication factors in response to nutritional conditions (***Droujinine and Perrimon, 2016***). We therefore hypothesized that, in larvae on LYD, C4da neurons receive signaling molecules from other tissues, leading to the hyperarborization via the Akt/Tor signaling pathway. As candidate receptors upstream of Akt, we focused on receptor tyrosine kinases (RTKs; ***Sopko and Perrimon, 2013***), and conducted C4da neuron-specific KD screenings of 20 RTK genes (***Supplementary file 2*** and ***Figure 2—figure supplements 4–6***; see 'RTK screening' in Materials and methods). One of the positive hits in our primary screening was *RTK-like orphan receptor* (*Ror*; ***Figure 2—figure supplement 4C and D***) and we confirmed that the *Ror* KD significantly suppressed the hyperarborization in the secondary screening (***Figure 2K–P***).

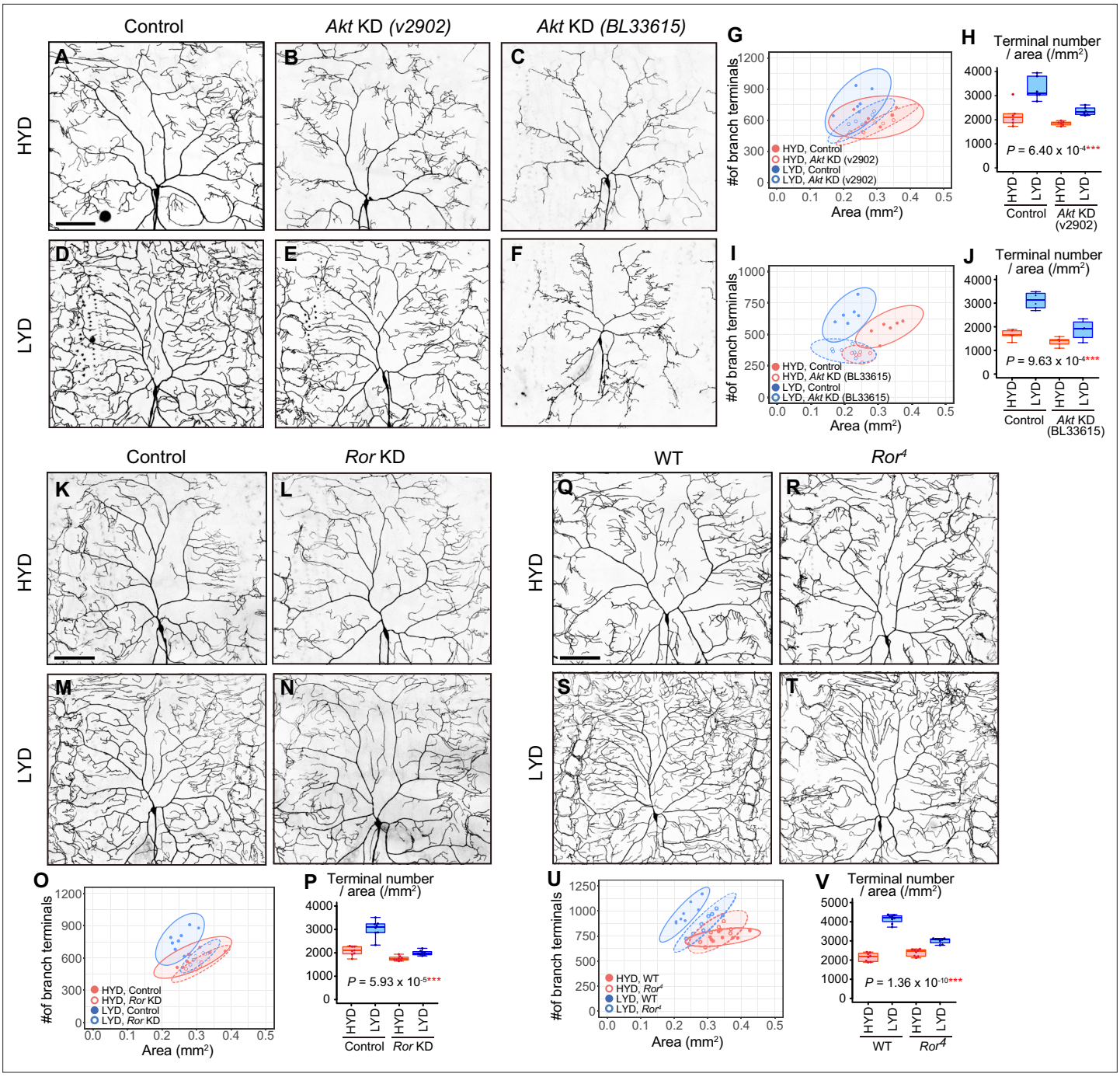

Figure 2. Akt and receptor tyrosine kinase Ror are required in C4da neurons to hyperarborize their dendrites. (**A–F**) Images of control ddaC neurons (**A and D**), or *Akt* knockdown (KD) ddaC neurons using *UAS-Akt RNAi*^{v2902} (**B and E**) or *UAS-Akt RNAi*^{BL33615} (**C and F**), on HYD (**A–C**) or LYD (**D–F**). (**G–J**) Quantitative analysis of effects of *Akt* KD using *UAS-Akt RNAi*^{v2902} (**G and H**) or *UAS-Akt RNAi*^{BL33615} (**I and J**). (**G and I**) 2D plots. (**H and J**) Densities of branch terminals. As indicated by the p-values, there was a significant interaction between diet and genotype on terminal density in both *Akt* KD experiments (two-way ANOVA, n=6). That is, compared to the difference between HYD and LYD in control C4da neurons, that difference in *Akt* KD neurons using *UAS-Akt RNAi*^{v2902} or *UAS-Akt RNAi*^{BL33615} was significantly smaller, suggesting that the hyperarborization was blunted by the *Akt* KD. (**K–P**) Images of control (**K and M**) or *Ror* knocked down ddaC (**L and N**) on HYD (**K and L**) or LYD (**M and N**). 2D plot (**O**) and densities of branch terminals (p, two-way ANOVA, n=8). (**Q–V**) Images of ddaC in wild-type (WT; **Q and S**) or *Ror*^{4} mutant larvae (**R and T**) on HYD (**Q and R**) or LYD (**S and T**). The ddaC neurons were visualized by expressing *ppk-CD4:tdGFP*. 2D plot (**U**) and densities of branch terminals (V, two-way ANOVA, n=8). Boxplots in (H, J, P, and V) are depicted as in ***Figure 1C***. ***p<0.001. Scale bars, 100 μm.

The online version of this article includes the following figure supplement(s) for figure 2:

Figure 2 continued on next page

Figure 2 continued

Figure supplement 1. Contributions of intracellular signaling factors or Akt signaling components to the hyperarborization.

Figure supplement 2. Roles of Akt and Ror in dendritic branching and elongation.

Figure supplement 3. Validation of knockdown efficiency of *Akt* RNAi lines and p-Akt antibody specificity.

Figure supplement 4. Results of the primary knockdown screening of RTK genes.

Figure supplement 5. Knockdown effects of *InR, Alk* or *htl* in the primary and the secondary screenings.

Figure supplement 6. RTK genes that were negative in the secondary screening.

Moreover, we observed C4da neurons in Ror^4 null mutant larvae and showed that they recapitulated the result of the KD (***Figure 2Q–V***). These results suggest that Ror and Akt are required in C4da neurons to hyperarborize their dendrites on LYD. Other positive hits included the known upstream regulators of Akt, Insulin-like receptor (InR) or Anaplastic lymphoma kinase (Alk). However, we could not definitively conclude whether InR and Alk contribute to the hyperarborization phenotype, due to inconsistent KD results among multiple experiments (***Supplementary file 2*** and ***Figure 2—figure supplement 5***).

To further characterize the phenotypes of the *Ror* KD and the v2902 *Akt* KD line, we measured the total length of branches per neuron (dendrite length) and dendrite length/area on each diet (***Figure 2—figure supplement 2A, B, E, F***). For both KD lines, values for length were higher on LYD compared to HYD in control C4da neurons. The v2902 line reduced dendrite length on both diets, although the decrease on HYD was marginal (***Figure 2—figure supplement 2A and B***), whereas *Ror* KD only decreased dendrite length on LYD (***Figure 2—figure supplement 2E and F***). This difference may reflect a restricted role for Ror in the response to a deficiency in the key nutrients, as opposed to a more general requirement of Akt for branch growth irrespective of the diets (***Figure 2—figure supplement 2G, H, J***).

Wg in muscles is more highly expressed on LYD and promotes dendritic branching of C4da neurons

Ror binds to Wnt ligands and triggers intracellular signaling cascades (***Ripp et al., 2018***; ***van Amerongen and Nusse, 2009***). We therefore knocked down *wingless* (*wg*), *Wnt2*, *Wnt4*, or *Wnt5* in either of the two tissues adjacent to C4da neurons: epidermal cells and muscles. We observed that *wg* KD in muscles using either *Mhc-GAL4* or *mef2-GAL4* suppressed the hyperarborization phenotype (***Figure 3A–F*** and ***Figure 3—figure supplement 1A–F***). In contrast, epidermal KD of *wg* had no effect on the phenotype (***Figure 3—figure supplement 1G–L***). The requirement of Wg for the hyperarborization was further confirmed by the finding that the hyperarborization effect was dampened in C4da neurons in the whole-body *wg* mutant (hypomorphic wg^1/amorphic $wg^{l\text{-}8}$; ***Figure 3G–L***).

We then examined whether Wg is differentially expressed in muscles between larvae reared on HYD and those on LYD. Immunostaining using an anti-Wg antibody showed stronger signals in LYD-fed larvae (***Figure 3M, N and P***). These stronger signals indeed represented increased amounts of endogenous Wg because knocking down *wg* decreased the intensity (***Figure 3—figure supplement 1M–Q***). We also asked whether *wg* expression is up-regulated on LYD at the transcriptional level. We expressed RedStinger, DsRed tagged with a nuclear localization signal, under the knocked-in *wg-GAL4* driver that reflects the endogenous expression pattern of *wg* (***Bosch et al., 2020***). Nuclear RedStinger signals in muscles were stronger in larvae on LYD (***Figure 3Q-S***), indicating that LYD up-regulated *wg* transcription compared to HYD. We further tested whether muscle-derived Wg promotes dendritic branching of C4da neurons. For this purpose, we overexpressed *wg* in muscles and found that those larvae increased the number of dendritic terminals per neuron on both HYD and LYD (***Figure 3T–Y***), strengthening the role of the muscle–C4da neuron communication in hyperarborization. Importantly, addition of vitamins, metal ions, and cholesterol to LYD significantly suppressed the up-regulation of Wg on LYD (***Figure 3M-P***). Together with the effect of these compounds on dendritic branching (***Figure 1S-U***), we hypothesized that *wg* expression in muscles is enhanced by a concurrent deficiency in vitamins, metal ions, and cholesterol in LYD, and that muscle-derived Wg promotes dendritic branching of C4da neurons.

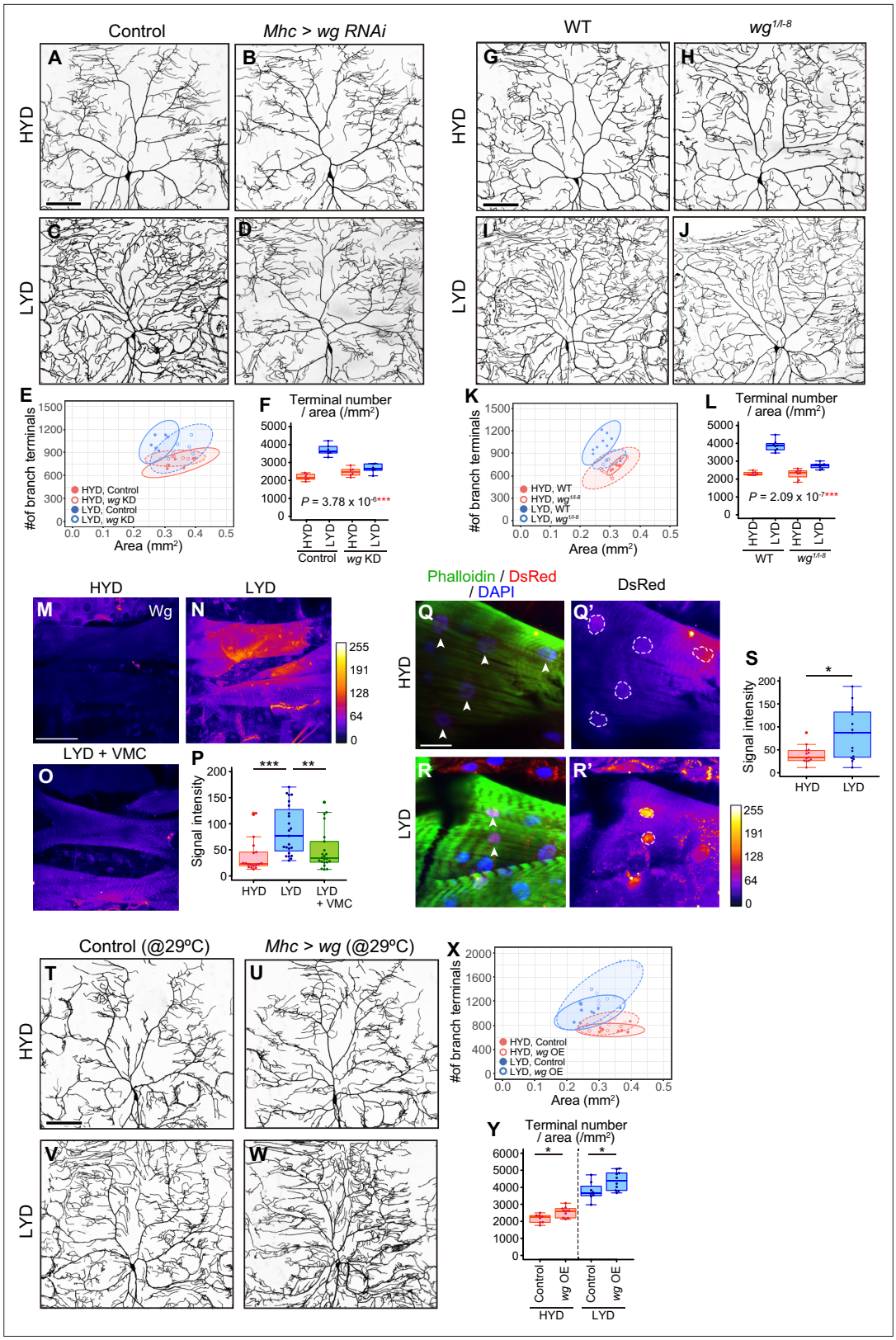

Figure 3. Wg in muscles is expressed more highly on LYD and promotes dendritic branching of C4da neurons. (**A–F**) Images of ddaC neurons in control larvae (**A and C**) or larvae with *wg* KD in muscles (**B and D**), on HYD or LYD. 2D plot (**E**) and densities of branch terminals (F, two-way ANOVA, n=6). (**G–L**) Images of ddaC neurons in WT (**G and I**) or $wg^{1/l\text{-}8}$ larvae (**H and J**) on HYD or LYD. 2D plot (**K**) and densities of branch terminals (L, two-way ANOVA,

Figure 3 continued on next page

Figure 3 continued

n=8). (**M–P**) Muscles in larvae reared on HYD (**M**), LYD (**N**), or LYD +VMC (**O**) were stained for Wg. The signal intensities are represented by the indicated color code. (**P**) Quantification of the mean Wg immunofluorescence intensity in muscle 9, one of the closest muscles to the ddaC neuron (Steel Dwass test, n=18–23). (**Q–S**) Images of *wg-Gal4* muscles driving the expression of RedStinger, which is DsRed tagged with a nuclear localization signal. Muscles, on HYD (**Q**) or LYD (**R**) were stained with phalloidin (green), an antibody to DsRed (red), and DAPI (blue). The signal intensities of DsRed are represented by the indicated color code, and white dashed circles indicate outlines of nuclei (Q'and R'). (**S**) Quantification of DsRed intensity in nuclei of muscle 9 (Wilcoxon-Mann-Whitney test, n=13–15). (**T–Y**) Images of ddaC neurons in control larvae (**T and V**) or larvae with *wg* overexpression at 29 °C in muscles (**U and W**) on HYD or LYD. 2D plot (**X**) and densities of branch terminals (Y, Wilcoxon-Mann-Whitney test, n=8–10). Experiments were couducted at both 29°C and 25°C, but only results at 29 °C are shown. At 29 °C, the effect of *wg* overexpression was expected to be higher, and in fact, branch terminal density increased on both HYD and on LYD, but only on HYD at 25 °C. The increase in the branch terminal density elicited by *wg* overexpression on both diets was less dramatic than the difference in the branch terminal density due to the diets in each respective genotype. The ddaC neurons were visualized by expressing *ppk-CD4:tdGFP*. Boxplots in (F, L, P, S, and Y) are depicted as in ***Figure 1C***. *p<0.05, **p<0.01, and ***p<0.001. Scale bars, 100 μm (A-D, G-J, M-O, and T-W), 25 μm (**Q-R'**).

The online version of this article includes the following figure supplement(s) for figure 3:

Figure supplement 1. Wg from muscles, but not from epidermal cells, contributes to the hyperarboriztion phenotype.

Wg-Ror-mediated activation of Akt in C4da neurons evokes the hyperarborization

Wnt signaling is engaged in diverse contexts of neuronal development and regeneration (***Green et al., 2014***; ***He et al., 2018***; ***Endo and Minami, 2018***; ***Nye et al., 2020***; ***Weiner et al., 2020***). In a previous study in *Drosophila*, responses to dendrite injuries were investigated using class I da (C1da) and C4da neurons. This showed that Ror, a seven-pass transmembrane receptor Frizzled (Fz), and downstream components including Disheveled (Dsh) and Axin (Axn) are required for dendrite regeneration (***Nye et al., 2020***). We therefore examined whether these genes and other components of Wnt signaling affect the hyperarborization phenotype (***Figure 4—figure supplement 1*** and ***Figure 4—figure supplement 2***). Knocking down *fz2* significantly ameliorated the hyperarborization (***Figure 4—figure supplement 1A, C, D, F, H, J***). Not only *fz2* KD neurons, but also *fz2* null mutant neurons showed less prominent hyperarborization compared to the control neurons (***Figure 4—figure supplement 1K–P***). These results are consistent with the proposed function of Ror as a Wnt co-receptor with Fz2 (***Ripp et al., 2018***). In addition to *fz2*, KD of *fz*, KD of downstream components (*dsh* and *Axn*), or expression of a dominant-negative form of Bsk also significantly blunted the hyperarborization (***Figure 4—figure supplement 1B, E, G, I*** and ***Figure 4—figure supplement 2*** [B, I, O and U], [G, N, T and Z], and [C, J, P and V]). However, we question whether all of these ameliorated phenotypes share the same underlying mechanism with those of *Ror* or *fz2* KD (see the legend of ***Figure 4—figure supplements 1 and 2***, and DISCUSSION). Altogether, our results suggest that among the known components of Wnt signaling in *Drosophila*, at least Fz2 cooperates with Ror in transducing the external signal to evoke the hyperarborization.

Ror is also reported to activate the PI3K/Akt/mTor signaling pathway in lung adenocarcinoma or multiple myeloma (***Liu et al., 2015***; ***Frenquelli et al., 2020***). We therefore hypothesized that Wg-Ror signaling activates Akt signaling in C4da neurons on LYD, leading to the hyperarborization. To test this hypothesis and to clarify the relationship between Wg-Ror and Akt at the molecular level, we examined how genetic manipulations of Wg-Ror signaling affect Akt activity levels in C4da neurons (***Figure 4A–J***). The specificity of the p-Akt antibody in C4da neurons was validated in two ways: (1) p-Akt signals were significantly reduced by *Akt* KD ***Figure 2—figure supplement 3A-H***; (2) expression of myr-Akt, a constitutively activated membrane-anchored form of Akt (***Stocker et al., 2002***), dramatically increased the p-Akt signal strength (***Figure 2—figure supplement 3I and J***). Using this antibody, we first examined how the p-Akt level in C4da neurons differs between larvae reared on HYD and LYD. Immunostaining showed that the p-Akt level in C4da neurons was higher on LYD than on HYD (***Figure 4A, A', C, C' , and E***). In contrast, *Ror* KD neurons from larvae on LYD showed reduced p-Akt levels compared to those on HYD (***Figure 4B, B', D, D' , and E***). Furthermore, *wg* overexpression

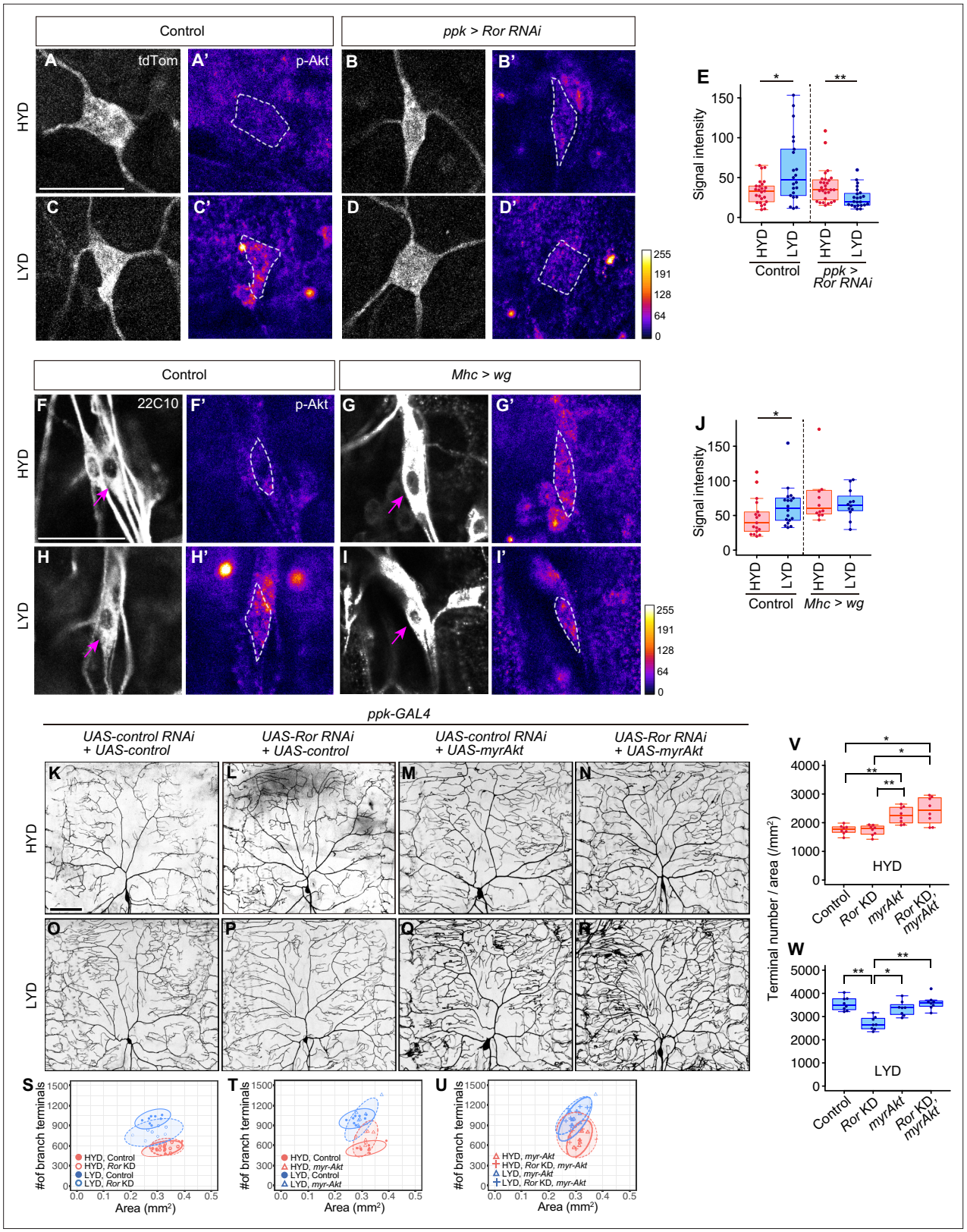

Figure 4. Wg-Ror-mediated activation of Akt in C4da neurons evokes the hyperarborization. (**A–E**) Control ddaC (**A, A', C and C'**) or *Ror* KD ddaC neurons (**B, B', D and D'**) were stained for p-Akt (**A'-D'**) and co-imaged with a C4da neuron marker *ppk-CD4:tdTom* (**A–D**). The signal intensities of p-Akt correspond to the indicated color code, at right, and white dashed circles indicate the cell bodies of ddaC neurons. (**E**) Quantification of p-Akt intensity in cell bodies of control or *Ror* knocked down ddaC neurons (Wilcoxon-Mann-Whitney test, n=22–28). (**F–J**) ddaC in control larvae (**F, F', H and H'**) or

Figure 4 continued on next page

Figure 4 continued

larvae with *wg* overexpression in muscles (**G, G', I and I'**) were stained for a pan-sensory neuron marker (22C10; **F–I**) and for p-Akt (**F'-I'**). (**F–I**) Magenta arrows indicate the cell bodies of ddaC neurons. (**F'-I'**) The intensities of p-Akt signals correspond to the indicated color code, at right, and white dashed circles indicate the cell bodies of ddaC neurons. (**J**) Quantification of p-Akt intensity in control larvae or larvae with *wg* overexpression in muscles (Wilcoxon-Mann-Whitney test, n=12–18). (**K–U**) Images of *UAS-control RNAi* and *UAS-control* expressing ddaC neurons (**K and O**), *UAS-Ror RNAi* and *UAS-control* expressing ddaC neurons (**L and P**), *UAS-control RNAi* and *UAS-myrAkt*, a constitutively active form of Akt, expressing ddaC neurons (**M and Q**), or *UAS-Ror RNAi* and *UAS-myrAkt* expressing ddaC neurons (**N and R**), on HYD or LYD. We used *UAS-grnd RNAi*, which had no significant impact on the hyperarborization phenotype (***Figure 2—figure supplement 1A and E***, 1I, and 1 M), as the *UAS-control RNAi* and *UAS-CD4:tdTom* as the *UAS-control*. (**S–W**) Quantitative analysis of combinatorial effects of *Ror* KD and *myrAkt* expression. (**S–U**) 2D plots. (**V and W**) Densities of branch terminals on HYD (**V**) or LYD (**W**) (Steel Dwass test, n=8–9). Boxplots in (**E, J, V and W**) are depicted as in ***Figure 1C***. *p<0.05 and **p<0.01. Scale bars, 25 μm (**A-D' and F-I'**), 100 μm (**K–R**).

The online version of this article includes the following figure supplement(s) for figure 4:

Figure supplement 1. Fz2, a receptor for Wnt proteins, is required in C4da neurons to hyperarborize their dendrites.

Figure supplement 2. Effects of inhibiting intracellular Wnt signaling components on hyperarborization.

Figure supplement 3. C3da neurons increased the number of dendrite terminals and p-Akt levels on LYD, while C1da neurons did not.

in muscles increased the p-Akt level in C4da neurons on HYD (compare ***Figure 4F'*** with 4 G'), which became comparable to the level on LYD (compare ***Figure 4G'*** with ***Figure 4I'***; see quantification in ***Figure 4J***). These results suggest that Akt signaling in C4da neurons is activated by muscle-derived Wg, and this activation is mediated by Ror in the neurons.

We further examined whether the activation of Akt itself evokes hyperarborization even in the absence of the upstream Ror-mediated signaling (***Figure 4K–W***). Expression of myr-Akt in C4da neurons increased the terminal density even on HYD, regardless of whether *Ror* was knocked down or not (compare ***Figure 4K*** with 4 M and 4 N; see also 4T, 4 U and 4 V). This result suggests that Akt activation in the neurons plays a pivotal role for the hyperarborization. Our result is consistent with a previous finding that overexpression of the wild-type form of *Akt* causes a significant increase in dendrite coverage of the epidermis (***Parrish et al., 2009***).

Somatosensation of *Drosophila* larvae depends on C4da and 3 other classes of da neurons. Among them, class I da (C1da) and class III da (C3da) neurons function in proprioception and gentle-touch sensation, respectively (***Hughes and Thomas, 2007***; ***Hwang et al., 2007***; ***Im and Galko, 2012***; ***Yan et al., 2013***; ***Tsubouchi et al., 2012***). We also examined whether the hyperarborization phenotype and p-Akt upregulation are observed in these classes. We previously reported that the hyperarborization phenotype is not seen in ddaD and ddaE C1da neurons (***Watanabe et al., 2017***). The p-Akt level showed no significant difference between HYD and LYD in ddaE neurons (***Figure 4—figure supplement 3A–C***). On the other hand, a C3da neuron, ddaF, showed an increase in both the dendritic terminal number and the p-Akt level on LYD (***Figure 4—figure supplement 3D–I***), similar to C4da neurons. Increased branch terminals of C3da neurons on a low-yeast diet was also reported previously (***Poe et al., 2020***). Our results raise the possibility that, along with C4da neurons, C3da neurons share the Akt-driven branching mechanism in response to the low-nutrient condition.

Stat92E partially contributes to downregulation of Wg expression and suppresses hyperarborization on HYD

Given that Wg expression in muscles is higher on LYD (***Figure 3M–P***), and the differential expression impacts the dendritic branching of C4da neurons (***Figure 3T–Y***), we then asked how Wg expression in muscles is regulated in the nutrient-dependent manner. To search for upstream regulators of the Wg expression, we performed RNA-seq analysis on mature whole larvae that were reared on either diet. We identified 3854 differentially expressed genes between the diets (***Figure 5A***, ***Figure 5—figure supplement 1***, and ***Supplementary file 3***). Among these, we focused on a transcriptional factor in the JAK/STAT pathway, *Stat92E*, which is more highly expressed on HYD than LYD (***Figure 5B***). Also informing our decision, it was reported that Stat92E is a negative regulator of *wg* expression in the eye imaginal disc (***Ekas et al., 2006***). We used a Stat92E reporter strain (***Bach et al., 2007***) and found that Stat92E reporter expression in muscle was higher on HYD (***Figure 5C–E***). We therefore hypothesized that, in muscles of larvae on HYD, higher expression of Stat92E downregulates Wg expression, thereby suppressing the hyperarborization phenotype. To test this hypothesis, we knocked down *Stat92E* in muscles, and this led to increased Wg levels compared to the control muscles on

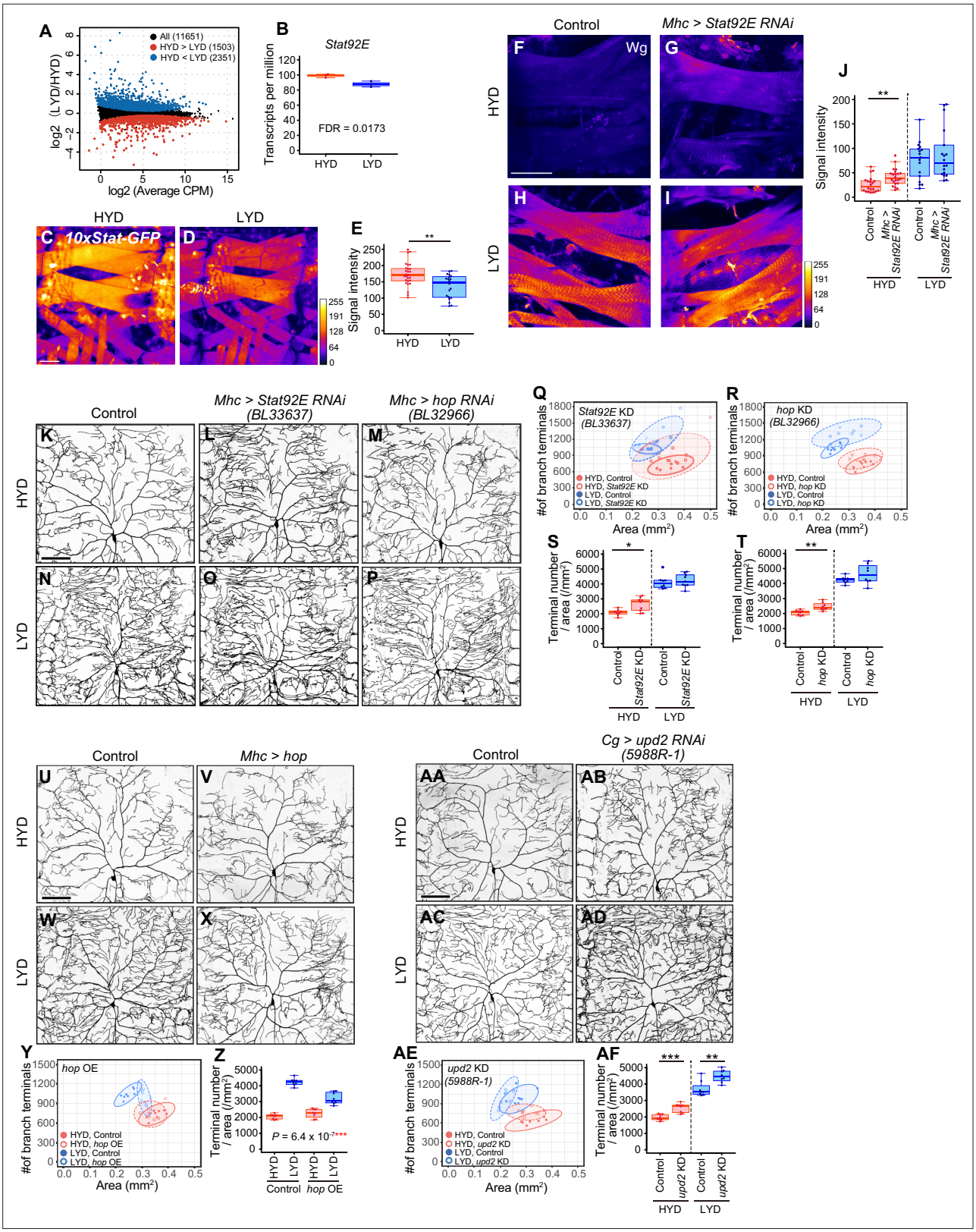

Figure 5. Downregulation of Wg expression by Stat92E on HYD suppresses the hyperarborization phenotype. (**A and B**) Plots of whole-body RNA-seq of wandering 3rd instar larvae reared on HYD or LYD. (**A**) The fold change (LYD/HYD) in read counts was plotted against average counts per million mapped reads (CPM) for HYD and LYD. Dots that are statistically supported (FDR ≤0.05) are colored (red for HYD >LYD and blue for HYD <LYD). (**B**) Plot of transcripts per million (TPM) of *Stat92E*. Adjusted p-value with Benjamini & Hochberg correction (FDR) is indicated. (**C–E**) Muscles of *10 x Stat-GFP*

Figure 5 continued on next page

Figure 5 continued

larvae on HYD (**C**) or LYD (**D**). The signal intensities of GFP correspond to the indicated color code. (**E**) Quantification of 10 x Stat-GFP intensity in muscle 9 (Student's t-test, n=20–27). (**F–J**) Muscles of control larvae (**F and H**) or larvae with *Stat92E* KD in muscles (**G and I**) on HYD or LYD were stained for Wg. The signal intensities correspond to the indicated color code. (**J**) Quantification of the mean Wg immunofluorescence in muscle 9 (Wilcoxon-Mann-Whitney test, n=17–22). (**K–T**) Images of ddaC neurons in control larvae (**K and N**), larvae with *Stat92E* KD in muscles (**L and O**), or larvae with *hop* KD in muscles (**M and P**), on HYD or LYD. 2D plots (**Q and R**) and densities of branch terminals (S and T, Wilcoxon-Mann-Whitney test, n=8–9). (**U–Z**) Images of ddaC neurons in control larvae (**U and W**) or larvae with *hop* overexpression in muscles (**V and X**), on HYD or LYD. 2D plot (**Y**) and densities of branch terminals (Z, two-way ANOVA, n=8). (AA-AF) Images of ddaC neurons in control larvae (AA and AC) or larvae with *upd2* KD in the fat body and hemocytes (AB and AD), raised on HYD or LYD. 2D plot (AE) and densities of branch terminals (AF, Wilcoxon-Mann-Whitney test, n=8). The ddaC neurons were visualized by expressing *ppk-CD4:tdGFP*. Control data in (**R**) and (**T**) are shared with (**Y**) and (**Z**). Boxplots in (**B, E, J, S, T, Z and AF**) are depicted as in ***Figure 1C***. *p<0.05, **p<0.01, and ***p<0.001. Scale bars, 100 μm.

The online version of this article includes the following figure supplement(s) for figure 5:

Figure supplement 1. Enriched terms in functional annotation clustering of differentially expressed genes depending on diets in whole body RNA-seq data.

Figure supplement 2. Effects of inhibiting components of JAK/STAT pathway on hyperarborization.

HYD (***Figure 5F–J***; compare 5 F with 5 G). Furthermore, knocking down *Stat92E* or *hopscotch* (*hop*) encoding JAK in muscles promoted hyperarborization of C4da neurons in larvae reared on HYD (***Figure 5K–T*** and ***Figure 5—figure supplement 2A, B, F, G, K, O***). In contrast, overexpression of *hop* in muscles ameliorated the hyperarborization on LYD (***Figure 5U–Z***). These results indicate that JAK/STAT signaling contributes to the downregulation of *wg* expression in muscles and the suppression of dendritic hyperarborization on HYD (Figure 7).

It was previously reported that Upd2 secreted from the fat body activates JAK/STAT signaling through transmembrane receptor Domeless (Dome) in GABAergic neurons in the adult brain, which project onto insulin producing cells (IPCs), thereby regulating systemic growth in a nutritional-status-dependent manner (***Rajan and Perrimon, 2012***). It has also been shown that the secretion of Upd2 or Upd3 from hemocytes promotes the expression of a Stat92E reporter in larval muscle (***Yang et al., 2015***). These studies prompted us to address whether any Upds from the fat body or hemocytes, and Dome in muscles, contribute to the hyperarborization phenotype. Knocking down *upd2,* but not *upd* or *upd3,* in the fat body and hemocytes resulted in an increased terminal density on HYD (***Figure 5AA-AF*** and ***Figure 5—figure supplement 2S-AN***). This effect of *upd2* KD in the fat body and hemocytes is similar to that of *Stat92E* or *hop* KD (***Figure 5K–T***) and that of *wg* overexpression in muscles (***Figure 3T–Y***). Enhanced branching on HYD was also seen in a *dome* KD in one out of three RNAi lines (***Figure 5—figure supplement 2C–E, H-J, L-N and P-R***). Although it is necessary to verify KD of *dome* in the future, these results are suggestive of the role of fat body (and hemocytes)–muscle inter-organ communication through a Upd2-Stat92E pathway in suppressing the hyperarborization phenotype on HYD. To address whether the key nutrients (vitamins, metal ions, and cholesterol) increase Stat92E expression in muscles, we examined the reporter expression on LYD supplemented with or without VMC. However, the addition of VMC to LYD did not increase the signal intensity of the Stat92E reporter (data not shown). This result contrasts with the decreased level of Wg in response to the key nutrients (***Figure 3M–P***). The *Stat92E* KD caused only a marginal Wg increase on HYD compared to the difference in the amount of Wg between HYD and LYD (***Figure 5F, H and J***). Considering these results, it is likely that an additional unknown molecular mechanism other than the JAK/STAT pathway contributes to the high VMC-mediated downregulation of Wg in muscles (Figure 7).

LYD blunts light responsiveness of C4da neurons and larval light avoidance behavior

C4da neurons sense noxious thermal, mechanical, and light stimuli (***Chin and Tracey, 2017***). We therefore examined how our dietary conditions affect the electrophysiological activity of C4da neurons and larval behavior (***Figure 6***). First, we compared firing activities of C4da neurons in larvae that were reared on either HYD or LYD. As a noxious stimulus, we illuminated entire arbors of recorded neurons with blue light (***Xiang et al., 2010***; ***Terada et al., 2016***). We used extracellular recording to monitor both spontaneous and evoked activities (***Figure 6A–C***). The frequency of spontaneous firing was higher in C4da neurons from larvae reared on LYD than on HYD (***Figure 6D***). Regarding the response to the light stimulus, all relevant parameters, i.e., the firing frequency, the change amount, and the

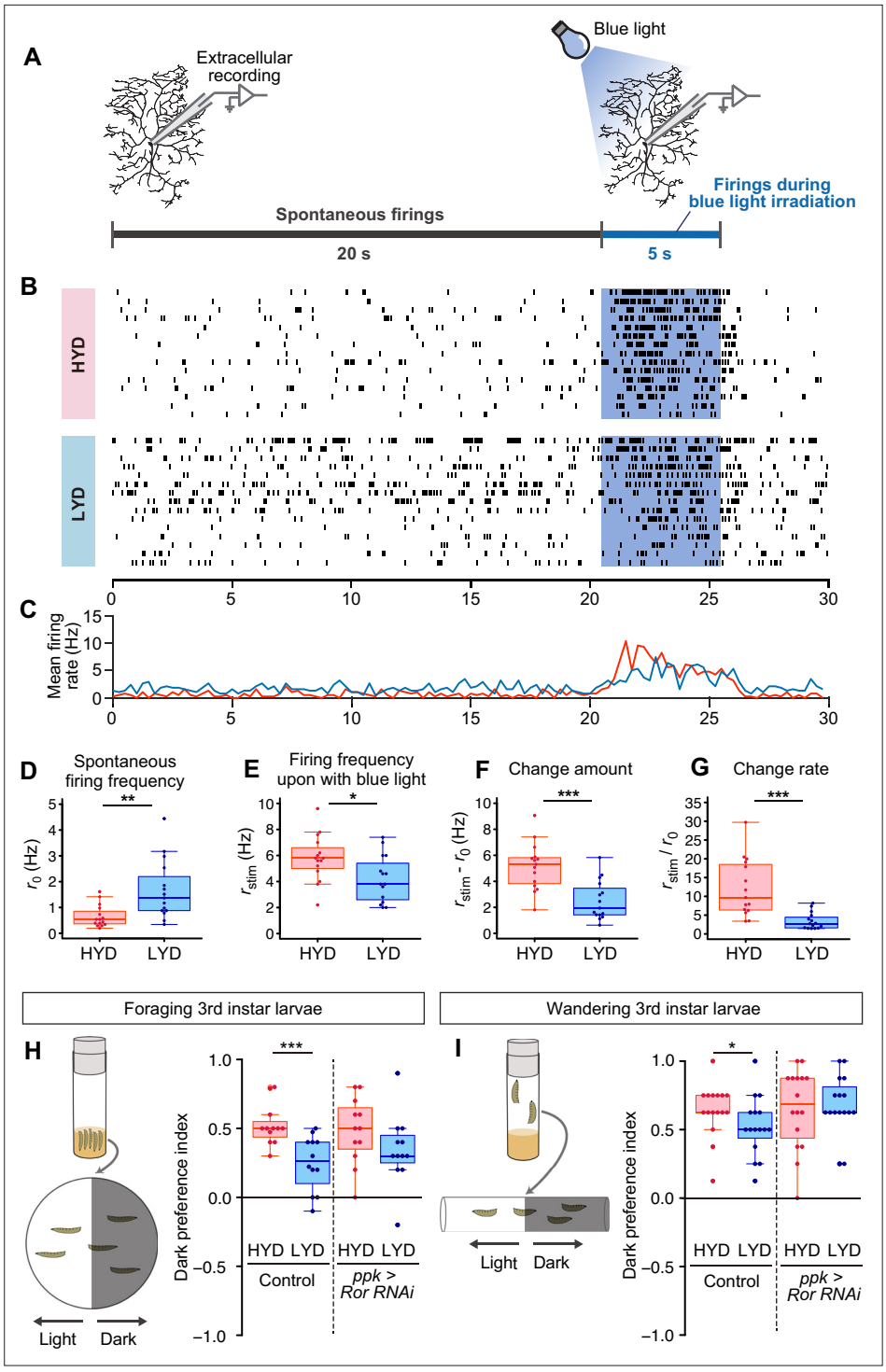

Figure 6. LYD blunts light responsiveness of C4da neurons and larval light avoidance behavior. (**A**) A schematic diagram outlining the electrophysiological analysis. Firing activities of C4da neurons v'ada were recorded by measuring the extracellular membrane potential. After spontaneous firings were recorded for about 20 s, activities during blue light irradiation were monitored for 5 s. (**B and C**) Firing activities of C4da neurons on HYD or LYD. (**B**) Raster plots of firing. Blue shading indicates the 5 s blue light irradiation. Each row in the plots represents the data for a single cell. (**C**) Peristimulus time histograms calculated at 250 ms bins, on HYD (red line) or LYD (blue line). (**D–G**) Quantitative analysis of the firing activities. (**D**) Spontaneous firing frequency. (**E**) Firing frequency during blue light irradiation. (**F**) Change amount of the firing response to the blue light stimulus calculated by subtracting [spontaneous firing frequency] from [firing frequency during blue light irradiation] (**G**) Change rate of

Figure 6 continued on next page

Figure 6 continued

the firing response to the blue light stimulus calculated by dividing [firing frequency during blue light irradiation] by [spontaneous firing frequency]. (Wilcoxon-Mann-Whitney test, n=15). (**H and I**) Schematic diagram of light/dark choice assays and dark preference index of foraging 3rd instar larvae on agar plates (**H**), and wandering 3rd instar larvae in plastic tubes (**I**). Control larvae and larvae with *Ror* KD in C4da neurons were tested. (Wilcoxon-Mann-Whitney test, n=12–16) Boxplots in (**D–I**) are depicted as in ***Figure 1C***. *p<0.05, **p<0.01, and ***p<0.001.

change rate, were lower on LYD than on HYD (***Figure 6E–G***, see definition of the parameters in the legend), indicating that C4da neurons on LYD are less sensitive to the stimulus. Next, we examined whether the blunted light responsiveness of the neurons affects larval avoidance behavior. It was reported that *Drosophila* larvae prefer dark places to avoid noxious light, and this light avoidance behavior requires the activity of C4da neurons (***Yamanaka et al., 2013***; ***Imambocus et al., 2022***). We speculated that the blunted light responsiveness of larvae on LYD may cause declines in their light avoidance behavior, and this may allow larvae to continue their search for high-nutrient food. To address this possibility, we conducted light/dark choice assays in which larvae reared on HYD or LYD were allowed to choose between dark and bright areas. We found that both foraging 3rd instar

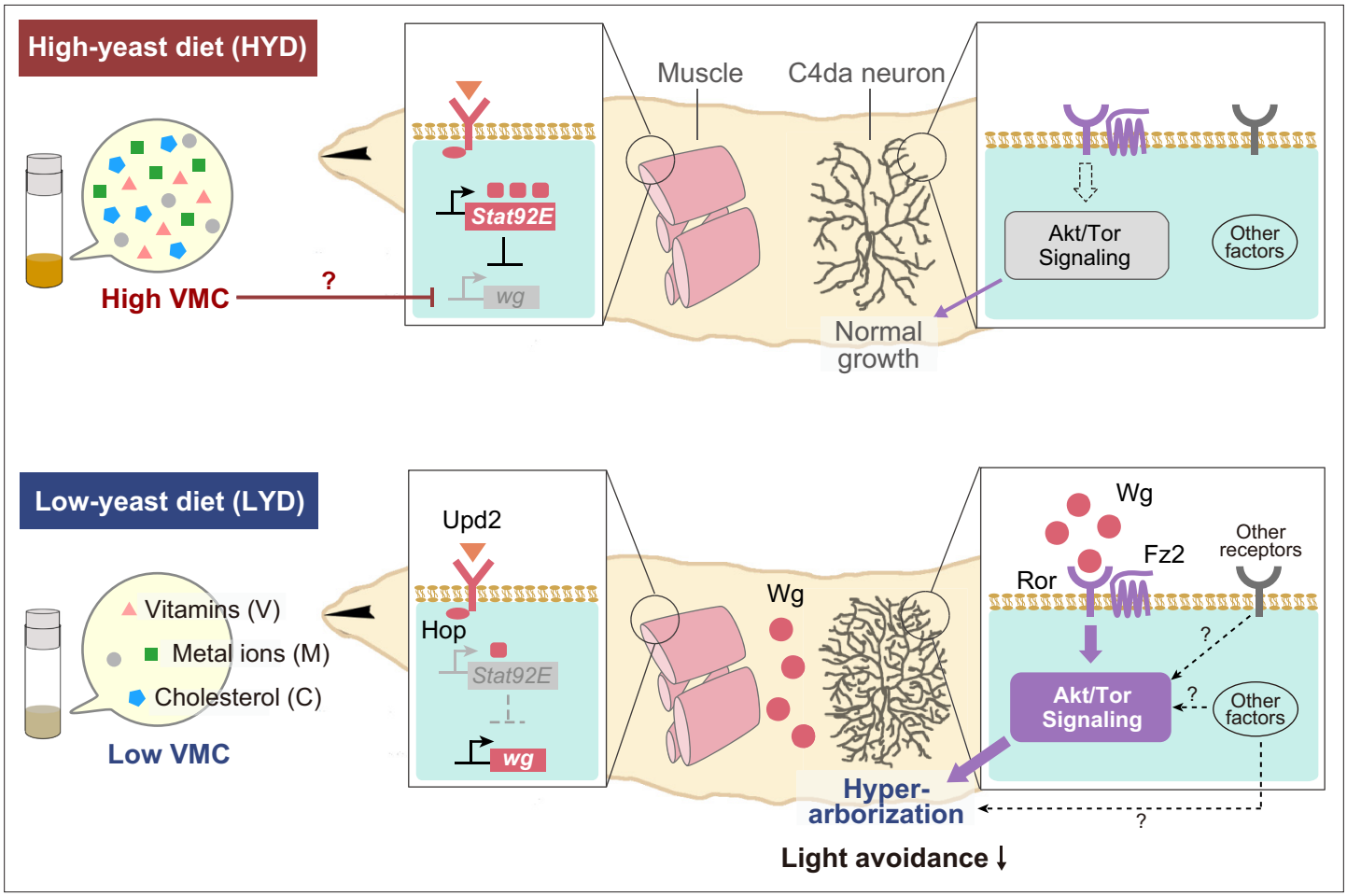

Figure 7. Model of the low-nutrient dependent dendritic hyperarborization. Compared to C4da neurons of HYD-fed larvae (top), those of LYD-fed larvae (bottom) increase in dendritic branching (hyperarborization) due to a combined deficiency of vitamins, metal ions, and cholesterol in the food ('Low VMC'). In the LYD-fed larvae, *wg* expression in muscles is higher than in muscles in the HYD-fed larvae; secreted Wg is bound by receptors Ror and Fz2 in C4da neurons, which in turn hyperactivate Akt signaling, thereby promoting dendrite branching. In the C4da neurons, other receptors (e.g. InR or Alk) upstream of Akt and intracellular components of Wnt signaling ('Other factors' such as Dsh and Bsk) might also contribute to the hyperarborization phenotype. The cellular response of C4da neurons is associated with a whole-animal level response (blunted light avoidance behavior). In the HYD-fed larvae, *wg* expression is suppressed partly by Upd2-Hop-Stat92E signaling and partly by an abundant VMC-mediated unknown molecular mechanism (red T bar and '?'). See Results and Discussion for details.

and wandering 3rd instar larvae on LYD showed lower preference for dark places than larvae on HYD (***Figure 6H and I***). Furthermore, when *Ror* was knocked down in C4da neurons, differences in light avoidance behavior between the diets tended to be smaller than the control larvae (***Figure 6H and I***). Our results suggest that the hyperarborization of C4da neurons is associated with blunted light avoidance behavior.

Discussion

Collectively, our studies illustrate how selective nutrients in the food impact neuronal development through inter-organ signaling (***Figure 7***). Yeast has long been considered as a rich source of amino acids for *Drosophila*; however, our results suggest that C4da neurons increase their dendritic terminal density on the LYD due to a combined deficiency in vitamins, metal ions, and cholesterol. This result is unexpected, because previous studies on nutrition-dependent cell growth has focused primarily on the TOR signaling pathway, which is activated by amino acids (***González et al., 2020***; ***Liu and Sabatini, 2020***). The addition of the above nutrient trio to LYD did not restore the branch terminal density to the same level as HYD. This may indicate that the balance of concentrations among these nutrients was not optimized or that unknown nutrients may need to be added along with these nutrients. In addition, we showed that up-regulation of Wg expression in muscle on LYD was suppressed by supplementation of these components to the diet. This regulation may be achieved at least at a transcriptional level possibly by an interplay between a hypothetical nutrient-responsive module in the cis-element of *wg* and transcription factors and/or epigenetic machineries that require vitamins, vitamin-derived metabolites, metal ions and cholesterol (***Harris et al., 2016***; ***Kambe et al., 2016***). Further investigations are necessary to understand the detailed molecular mechanisms underlying the combined effects of these components on *wg* expression. It has been reported that increasing or decreasing the amount of yeast in foods causes various responses in *Drosophila* (***Bass et al., 2007***; ***Okamoto and Nishimura, 2015***), and the approach used in this study may help to clarify which nutrients are the key factors that cause those responses.

Inter-organ Wg/Ror/Akt signaling-mediated the hyperarborization phenotype

Previous studies demonstrated the coordinate growth control of dendrites of C4da neurons and the epidermis (***Parrish et al., 2009***; ***Jiang et al., 2014***), from which a separate model underlying dendritic hyperarborization has evolved (***Poe et al., 2020***). In that model, stress sensor FoxO is expressed less in neurons than in neighboring epidermal cells, which results in lower levels of autophagy and less suppression of Tor signaling in the neuron, thereby ensuring dendritic growth even under a low-yeast condition (***Poe et al., 2020***). In contrast to the above model, our model highlights the signaling between neurons and another adjacent tissue: muscles secrete Wg, while C4da neurons express the receptor complex Ror-Fz2 on their cell surface. Therefore, it is likely that both the extrinsic Wg-dependent mechanism and the FoxO-dependent intrinsic sparing mechanism work together to generate the hyperarborization phenotype.

Ror is mainly expressed in the nervous system. No significant abnormalities in neuronal morphology including that of the C4da neurons were observed in *Ror* mutants under standard dietary conditions (***Ripp et al., 2018***; ***Nye et al., 2020***). Consistent with these reports, there was no significant difference in morphological features of dendritic arbors of C4da neurons between *Ror* mutant or KD larvae and control larvae under the nutrient-rich HYD condition (***Figure 2L and R***). Because Ror is required for the hyperarborization under the hypotrophic condition (LYD in this study; ***Figure 2N and T***) and for dendrite regeneration through the regulation of microtubule nucleation (***Nye et al., 2020***), it could be an adaptive agent that copes with environmental stress or damage. The pathway for microtubule nucleation includes Dsh and Axn, whose KD appeared to ameliorate the hyperarborization of C4da neurons. It remains to be seen how Dsh and Axn contribute to the hyperarborization on LYD, and whether the Wg-Ror-Akt pathway and the Ror-mediated microtubule-nucleation mechanism intersect. A number of other RTKs, such as insulin/IGF receptors and EGFR, activate Akt in other cellular contexts such as growth and proliferation of various stem cells and mammalian cancer cells (***Shim et al., 2013***; ***Butti et al., 2018***). It is likely that InR also functions upstream of Akt in C4da neurons (***Parrish et al., 2009***; ***Shimono et al., 2014***; ***Poe et al., 2020***). Future studies will explore whether InR

and other RTKs indeed function upstream of Akt in the context of the Wg/Ror/Akt signaling, and if so, how these various inputs are integrated by Akt to realize the nutritional status-dependent dendrite branching of C4da neurons (***Figure 7***).

The muscle is not only an energy-consuming organ, but it also plays an important role in regulating metabolic signaling through inter-organ communication with other tissues such as the brain and the fat body (***Bretscher and O'Connor, 2020***). In the adult stage, for example, muscle-derived Wg regulates lipid storage in the fat body (***Lee et al., 2014***). Our study revealed that muscle-derived Wg, which is up-regulated in response to low levels of vitamins, metal ions, and cholesterol, regulates dendrite branching of C4da neurons in the larval stage. Therefore, the muscle functions as a mediator of the nutritional status to other peripheral tissues in both growing and adult stages, and Wnt signaling may play a pivotal role in fulfilling this metabolic response function throughout the life cycle.

In our search for regulatory mechanisms of *wg* expression, we found that Stat92E reporter expression was higher in muscles on HYD than on LYD. This finding is reminiscent of Stat92E reporter expression in a population of GABAergic neurons in the adult brain, which project onto the Insulin producing cells (IPCs) and inhibit the release of Dilps (***Rajan and Perrimon, 2012***). This reporter expression in the GABAergic neurons also varies in a nutritional-status-dependent manner: the expression is higher on a standard laboratory food containing yeast compared to a sucrose-only condition. Our results suggest that Upd2-Stat92E signaling partially contributes to downregulation of Wg in muscles and suppression of the hyperarborization phenotype. When *stat92E* was knocked down in muscles, Wg increased on HYD; however, that increase was marginal compared to the difference in the level of Wg expression between HYD and LYD (***Figure 5F, G, H and J***). Moreover, the addition of a combination of vitamins, metal ions, and cholesterol to LYD did not increase the signal intensity of a Stat92E reporter (data not shown). Therefore, it is likely that in the HYD-fed larvae, an unknown VMC-mediated molecular mechanism also contributes to downregulation of *wg* in muscles (red T bar with '?' in ***Figure 7***). Further investigation is required to elucidate how Wg expression in muscles is controlled at the molecular level in such a key nutrient(s)-dependent manner and how the Upd2-Stat92E pathway contributes to the entire mechanism of inter-organ communication.

Physiological roles of C4da neurons and the hyperarborization phenotype

What are the implications of the inter-organ signaling mechanism controlling dendritic branches in the context of nutritional adaptation? It has been reported that a wide range of animals tend to take more risks when they are hungry (***Symmonds et al., 2010***; ***Filosa et al., 2016***; ***Padilla et al., 2016***; ***Bräcker et al., 2013***). Our electrophysiological analysis indicates that C4da neurons on LYD decrease light-evoked response (***Figure 6A–G***). Consistently, larvae reared on LYD displayed decreases in their dark preference, compared to those reared on HYD, and they explored bright places, which is potentially risky for their survival (Control of ***Figure 6H and I***). This difference between the diets tended to become smaller once the inter-organ signaling mechanism was suppressed in C4da neurons (*ppk >Ror* RNAi in ***Figure 6H and I***). These results imply that the hyperarborization of C4da neurons on LYD might contribute to blunting light avoidance behavior, although we cannot exclude the possibility that the *Ror* KD might affect neuronal functions through other mechanisms than the dendritic morphological change. Our study raises the possibility that nutrient-dependent development of somatosensory neurons plays a role in optimizing a trade-off between searching for high-nutrient foods and escaping from noxious environmental threats. Although a recent study described the circuitry required for the larval light avoidance behavior, it remains unclear whether the possible modifications of neural circuits downstream of C4da neurons take part in this behavioral transition (***Imambocus et al., 2022***). The identification of the downstream circuits would allow further study of the relationship between nutrient-dependent neural differentiations and evoking risk-taking behavior.

In contrast to our results, a previous study reported that larvae with hyperarborized C4da neurons react more quickly to noxious heat (***Poe et al., 2020***). While light-induced Ca^{2+} activity in C4da neurons decreases, thermal nociceptive behavior increases during 2nd and 3rd instar larval periods (***Jaszczak et al., 2022***), which indicates that these nociceptive responses are regulated in the opposite direction or in distinct fashions. Therefore, seemingly contradictory results between the previous study and ours may be due to different regulatory mechanisms of the sensory modalities.

The relationship between nutritional status and neural development has often been studied epidemiologically (**Prado and Dewey, 2014**; **Bhutta et al., 2017**). Our study, which presents a mechanism by which quantitative changes in specific nutrients act on neuronal morphology and operate through inter-organ signaling, provides a stepping stone for future explorations of molecular mechanisms linking nutrition and development of other neuronal cell types and in other animal species.

Materials and methods

Drosophila strains and fly culture

Fly strains used in this study are listed in Key Resources Table. Our stocks are usually reared on a laboratory standard diet (**Watanabe et al., 2017**). Adult males and virgin females that had developed on the standard diet were collected and crossed on the standard diet for 3–5 days. Then, the adults were transferred into vials containing HYD or LYD, which were identical to the semidefined medium (SDM)-based diet (8% Y) and the SDM-based diet (0.8% Y), respectively (see **Supplementary file 1** and its legend in **Watanabe et al., 2017**). After an egg-laying interval, the adult flies were cleared in every experiment and wandering 3rd instar larvae that came out of individual diets were used. Larvae were reared under noncrowded conditions at 25 °C in all the experiments except the *wg* overexpression experiments at 29 °C. Our recombinant DNA experiments follow Kyoto University Regulations for Safety Management in Recombinant DNA Experiments under protocol # 210059.

Experimental diets

We cooked the high yeast diet (HYD) or low yeast diet (LYD) based on semidefined media (SDM) as described previously (**Watanabe et al., 2017**). The original SDM recipe is described at the Bloomington *Drosophila* Stock Center https://bdsc.indiana.edu/information/recipes/germanfood.html. HYD and LYD were composed of brewer's yeast (MPBio 2903312), glucose (Wako 049–31165), sucrose (Wako 196–00015), peptone (Fluka 82303), and agar (Matsuki Kanten). The complete compositions of these diets can be found in **Supplementary file 1**. After the ingredients were mixed, water was added to a final volume of 200 ml, followed by autoclaving. Once the foods had cooled, 1.2 ml propionic acid (Nacalai Tesque, 29018–55) and 2 ml 10% butyl p-hydroxybenzoate (Nacalai Tesque, 06327–02) in 70% ethanol were added. The foods were then dispensed into vials and left overnight before use.

For the supplementation with essential amino acid solution, we used 50 x MEM EAA solution (Wako 132–15641). Each fraction of holidic medium (**Piper et al., 2014**; **Piper et al., 2017**) other than amino acids (vitamins, cholesterol, metal ion and other ingredients) was added to LYD at 10 times the concentration in holidic medium. Amino acids mixture from holidic medium was added at a 1 x or 3 x concentration. The complete compositions of diets used in nutrient supplementation experiments can be found in **Supplementary file 1**.

Imaging and quantification for assessing dendritic morphology

Images of ddaC (C4da) or ddaF (C3da) neurons in A3–A5 segments were acquired in live whole-mount larvae as described (**Hattori et al., 2013**; **Parrish et al., 2009**; **Matsubara et al., 2011**). Protocols for single-cell labeling (MARCM) were as previously described (**Shimono et al., 2014**). For quantification of the number of dendritic branching terminals, we drew an outline of the dendritic field as a region of interest (ROI) by connecting the outermost dendritic terminals with the Adobe Photoshop path tool. Then, dendritic branching terminals inside the ROI of ddaC were automatically counted using DeTerm (**Kanaoka et al., 2019**). Concerning counting short spikes of ddaF, results obtained by DeTerm were corrected manually. In addition, the area size of the ROI was measured as the dendritic coverage size. Dendrite length of ddaC neurons was measured using Fiji/ImageJ as previously described (**Poe et al., 2017**). Briefly, images of dendrites were processed sequentially by Gaussian Blur, Auto Local Threshold, Particles4, and Skeletonize (2D/3D), and the length of the 1-pixel-width skeleton was measured inside the ROI. Some representative control images and control data are shared by multiple figures. See figure legends.

Preparation of larvae with developmental delay

In the experiments in which larval growth was delayed by excess sucrose, we collected eggs as previously described (**Watanabe et al., 2019**) and placed them on either HYD, LYD, or HYD +sucrose in

vials. The complete composition of HYD + sucrose can be found in ***Supplementary file 1***. In a *dilp8* overexpression experiment (***Colombani et al., 2012***), the adult flies were allowed to oviposit on HYD or LYD for 24 hr. The timing of the neuronal observations under each condition is indicated in ***Figure 1—figure supplement 2***.

RTK screening

We conducted two rounds of screening. In the primary screening, we intended to enhance KD efficacy and used *Gr28b.c-GAL4* and *ppk-GAL4* together. We acquired images of 3–8 knocked-down neurons for each gene on each diet, and then visually judged whether hyperarborization was blunted or not. We selected nine genes (*Ror*, *InR*, *Alk*, *htl*, *Egfr*, *Pvr*, *Ddr*, *dnt*, and *drl*) for the secondary screening, in which we used only *ppk-GAL4* because *Gr28b.c-GAL4* is expressed in a small subset of neurons in the central nervous system in addition to C4da neurons in the peripheral nervous system (***Xiang et al., 2010***). See ***Supplementary file 2*** for names of the 20 RTK genes and stock numbers of RNAi lines used.

Immunostaining

Dissected wandering 3rd instar larvae were fixed in a 1:10 dilution of Formaldehyde Solution (Nacalai Tesque, 16222–65) in PBS plus 0.05% Triton X-100 for 30 min, then washed three times in PBS plus 0.1% Triton X-100 (PBST). After blocking in PBST plus 2% bovine serum albumin for 30 min, primary antibodies listed in Key Resources Table were added, then incubated overnight at 4 °C. After three successive washes, secondary antibodies were added, then incubated for 1 hr at room temperature. Finally, samples were mounted using FluorSave Reagent (Calbiochem). Most of the images were acquired with a Nikon C1 laser scanning confocal microscope coupled to a Nikon Eclipse E-800 microscope. The images in ***Figure 2—figure supplement 5*** were acquired with a ZEISS LSM 800 microscope.

Quantification of signal intensity

To quantify signal levels in muscle, we made Z-stack images and chose muscle 9, one of the closest muscles to ddaC, for measuring the signal intensity. For quantification of Wg or 10 x Stat-GFP signals, we measured the signal intensity inside a 19 μm or a 27 μm square ROI, respectively. Three ROIs were drawn for each muscle, and the average value was calculated. For quantification of RedStinger driven by *wg-GAL4*, the signal intensity inside nuclei that were identified by DAPI signals was measured. Then, the values from 2 to 7 nuclei in each muscle were averaged. For quantification of p-Akt levels in cell bodies of C4da ddaC, C1da ddaE or C3da ddaF neurons, we selected the single section containing the strongest signal in the neurons and measured signal intensities inside a 1.7 μm square ROI located on the abdominal side of nuclei of the neurons. However, for the quantification in ddaF neurons, the ROI was placed on the ventral side of nuclei only when we could not identify the border between ddaF and ddaC.

Electrophysiology

Extracellular single-unit recordings in wandering 3rd instar larvae were performed as previously described (***Terada et al., 2016***; ***Onodera et al., 2017***). We recorded the activity of v'ada of C4da neurons, which showed hyperarborization on LYD. For blue light irradiation, the 460–495 nm light at 72mW/mm^2 power was projected onto larvae for 5 s. The light spot was 1.5 mm in diameter. Peristimulus time histograms were calculated at 250 ms bins. The mean spontaneous firing frequencies were quantified in the 20 s window preceding the light stimuli. The mean firing frequencies during the light stimulation were quantified in the 5 s entire window. The firing changes were calculated by subtracting the mean spontaneous firing rate from the light-evoked one (Change amount) or using a ratio of the mean spontaneous firing rate divided by the mean light-evoked one (Change rate).

Light/dark choice assay

Light/dark choice assays were performed as previously described with modifications (***Yamanaka et al., 2013***). For the assay of foraging larvae, we used foraging 3rd instar larvae one day before they start wandering. We prepared 2% agar plate with a lid half of which was covered with black tape and 20 larvae were placed along the junction between light and dark sides. After the plates were illuminated

for 15 min with white LED light (OHM, ODS-LKL6-W) at 700 lux, the number of larvae in both dark and light areas were counted. In some trials, one or two larvae dug into the agar. Such larvae were excluded from calculation of dark preference index. For the assay of wandering larvae, two opposed plastic tubes were joined by transparent scotch tape and one of the vials was covered with black tape. After 16 wandering larvae reared on HYD or LYD were put near the junction of the tubes, they were illuminated by the 700 lux light for 15 min, then the number of larvae in both dark and light areas were counted. Dark preference index was calculated as follows:

$$\left(\left(\text{Number of larvae in dark}\right) - \left(\text{Number of larvae in light}\right)\right) / \left(\text{Total number of larvae}\right)$$

RNA-seq

Protocols for sample preparation and data analysis of RNA-seq were essentially as described in ***Watanabe et al., 2019***. To prepare each replicate, RNA was extracted from five whole bodies of male wandering third-instar larvae. The following procedures are different from ***Watanabe et al., 2019***: (1) the NEBNext Ultra II Directional RNA Library Prep Kit for Illumina (NEB, E7760) was used for library preparation. (2) RNA-sequencing was performed on an Illumina NextSeq 500 system using single end reads. (3) All raw sequencing data were trimmed using TrimGalore (ver. 0.6.0, Cutadapt ver. 1.18; DOI:10.5281/zenodo.5127899, DOI:10.14806/ej.17.1.200) with -clip_R1 13 option. (4) Gene-based read counts were obtained using htseq-count (ver. 0.11.3; ***Anders et al., 2015***) with -s reverse -a 10 options. (5) Differential expression analysis was performed on the count data using a generalized linear model (GLM) in the edgeR Bioconductor package (ver. 3.30.3; ***McCarthy et al., 2012***; ***Robinson et al., 2010***). All the RNA-sequencing data have been deposited and are available in the DDBJ Sequence Read Archive. The accession numbers for the data are DRR311224-DRR311229 (BioProject accession number: PRJDB12048).

Statistical analysis

R (R Core Team) was used for stastical analysis. Values of $P<0.05$ were considered statistically different. Student's t-test or the Wilcoxon-Mann-Whitney test was used for two-group comparisons, and Dunnett's test, Steel test, or Steel-Dwass tests were used for multiple comparisons. We used two-way analysis of variance (ANOVA) to analyze interactive effects between genotype and diet. On the other hand, we used the two-group comparison tests (Student's t-test or the Wilcoxon-Mann-Whitney test) when we simply focused on whether a genetic manipulation itself affected dendrite branching on the same diet. Statistical tests used, the exact sample size (n), and p values are shown in ***Supplementary file 4***. R was also used to draw 95% confidence ellipses. See also figure legends for details.

Acknowledgements

The reagents and genomic datasets were provided by the *Drosophila* Genetic Resource Center at Kyoto Institute of Technology, National Institute of Genetics, the Bloomington Stock Center, Vienna *Drosophila* Resource Center, FlyBase, and the Developmental Studies Hybridoma Bank maintained by the University of Iowa. We thank T Kondo and Y Sando for performing RNA-sequencing; J A Hejna for polishing the manuscript; T Kambe, R Niwa, T Jovanic, N Yamanaka, S Goulas, Y Shimada-Niwa, N Okamoto and other members of the Uemura laboratory for discussions and their technical assistance; M M Rolls, A Wodarz, T Igaki, T Ito, M Nakamura, M Yamazaki, M Sato, P Leopold, Y Sanaki and T Nishimura for kindly providing reagents; and Y Xiang for sharing unpublished results.

Additional information

Funding

Funder	Grant reference number	Author
Japan Agency for Medical Research and Development	JP18gm1110001	Tadashi Uemura

Funder	Grant reference number	Author
Japan Society for the Promotion of Science	15H02400	Tadashi Uemura
Japan Society for the Promotion of Science	21H00251	Yukako Hattori
Japan Society for the Promotion of Science	21K06186	Yukako Hattori
Japan Society for the Promotion of Science	20J15084	Yasutetsu Kanaoka
Japan Science and Technology Agency	JPMJFR2051	Yukako Hattori
Naito Foundation		Yukako Hattori
Japan Foundation for Applied Enzymology		Yukako Hattori

The funders had no role in study design, data collection and interpretation, or the decision to submit the work for publication.

Author contributions

Yasutetsu Kanaoka, Resources, Data curation, Formal analysis, Funding acquisition, Investigation, Visualization, Methodology, Writing – original draft; Koun Onodera, Data curation, Formal analysis, Investigation, Visualization, Methodology, Writing – review and editing; Kaori Watanabe, Investigation, Methodology, Writing – review and editing; Yusaku Hayashi, Investigation; Tadao Usui, Methodology, Writing – review and editing; Tadashi Uemura, Conceptualization, Resources, Supervision, Funding acquisition, Methodology, Writing – original draft, Project administration, Writing – review and editing; Yukako Hattori, Conceptualization, Data curation, Formal analysis, Supervision, Funding acquisition, Investigation, Visualization, Methodology, Writing – original draft, Project administration, Writing – review and editing

Author ORCIDs

Yasutetsu Kanaoka http://orcid.org/0000-0002-1835-3248
Koun Onodera http://orcid.org/0000-0002-4203-9865
Kaori Watanabe http://orcid.org/0000-0003-2887-3690
Tadao Usui http://orcid.org/0000-0002-0507-1495
Tadashi Uemura http://orcid.org/0000-0001-7204-3606
Yukako Hattori http://orcid.org/0000-0001-5977-8501

Ethics

Our recombinant DNA experiments follow Kyoto University Regulations for Safety Management in Recombinant DNA Experiments under protocol # 210059.

Decision letter and Author response

Decision letter https://doi.org/10.7554/eLife.79461.sa1
Author response https://doi.org/10.7554/eLife.79461.sa2

Additional files

Supplementary files

- Supplementary file 1. Compositions of the experimental diets.
- Supplementary file 2. Summary of the RTK knockdown screening.
- Supplementary file 3. RNA-seq data of larval whole bodies at the wandering third-instar stage on HYD or LYD. (A) List of Differentially expressed genes between HYD and LYD in whole larval bodies at the wandering third-instar stage (adjusted P value < 0.05). (B and C) List of functional annotation clusters that were significantly enriched (enrichment score ≥ 1.3) in genes highly expressed on HYD rather than on LYD (B) or genes highly 1385 expressed on LYD rather than on HYD (C).
- Supplementary file 4. Statistical details of experiments and a list of genotypes.

- MDAR checklist

Data availability

All the RNA-sequencing data have been deposited and are available in the DDBJ Sequence Read Archive. The accession numbers for the data are DRR311224-DRR311229 (BioProject accession number: PRJDB12048).

The following dataset was generated:

Author(s)	Year	Dataset title	Dataset URL	Database and Identifier
Hattori Y, Kanaoka Y, Uemura T	2021	Transcriptome analysis of male *Drosophila* larvae reared on two different diets	https://ddbj.nig.ac.jp/resource/sra-submission/DRA012492	DDBJ Sequence Read Archive, DRR311224-DRR311229

References

Anders S, Pyl PT, Huber W. 2015. HTSeq--a python framework to work with high-throughput sequencing data. *Bioinformatics* **31**:166–169. DOI: https://doi.org/10.1093/bioinformatics/btu638, PMID: 25260700

Bach EA, Ekas LA, Ayala-Camargo A, Flaherty MS, Lee H, Perrimon N, Baeg GH. 2007. GFP reporters detect the activation of the *Drosophila* JAK/STAT pathway in vivo. *Gene Expression Patterns* **7**:323–331. DOI: https://doi.org/10.1016/j.modgep.2006.08.003

Bass TM, Grandison RC, Wong R, Martinez P, Partridge L, Piper MDW. 2007. Optimization of dietary restriction protocols in *Drosophila*. *The Journals of Gerontology. Series A, Biological Sciences and Medical Sciences* **62**:1071–1081. DOI: https://doi.org/10.1093/gerona/62.10.1071, PMID: 17921418

Bhutta ZA, Berkley JA, Bandsma RHJ, Kerac M, Trehan I, Briend A. 2017. Severe childhood malnutrition. *Nature Reviews. Disease Primers* **3**:17067. DOI: https://doi.org/10.1038/nrdp.2017.67, PMID: 28933421

Bosch JA, Colbeth R, Zirin J, Perrimon N. 2020. Gene knock-ins in *Drosophila* using homology-independent insertion of universal donor plasmids. *Genetics* **214**:75–89. DOI: https://doi.org/10.1534/genetics.119.302819, PMID: 31685521

Bräcker LB, Siju KP, Varela N, Aso Y, Zhang M, Hein I, Vasconcelos ML, Grunwald Kadow IC. 2013. Essential role of the mushroom body in context-dependent CO_2 avoidance in *Drosophila*. *Current Biology* **23**:1228–1234. DOI: https://doi.org/10.1016/j.cub.2013.05.029, PMID: 23770186

Bretscher H, O'Connor MB. 2020. The role of muscle in insect energy homeostasis. *Frontiers in Physiology* **11**:580687. DOI: https://doi.org/10.3389/fphys.2020.580687, PMID: 33192587

Butti R, Das S, Gunasekaran VP, Yadav AS, Kumar D, Kundu GC. 2018. Receptor tyrosine kinases (rtks) in breast cancer: signaling, therapeutic implications and challenges. *Molecular Cancer* **17**:34. DOI: https://doi.org/10.1186/s12943-018-0797-x, PMID: 29455658

Chantranupong L, Wolfson RL, Sabatini DM. 2015. Nutrient-Sensing mechanisms across evolution. *Cell* **161**:67–83. DOI: https://doi.org/10.1016/j.cell.2015.02.041, PMID: 25815986

Chen CM, Struhl G. 1999. Wingless transduction by the frizzled and FRIZZLED2 proteins of *Drosophila*. *Development* **126**:5441–5452. DOI: https://doi.org/10.1242/dev.126.23.5441

Chin MR, Tracey WD. 2017. Nociceptive circuits: Ca ''t escape detection. *Current Biology* **27**:R796–R798. DOI: https://doi.org/10.1016/j.cub.2017.07.031

Colombani J, Andersen DS, Léopold P. 2012. Secreted peptide dilp8 coordinates *Drosophila* tissue growth with developmental timing. Science **336**:582–585. DOI: https://doi.org/10.1126/science.1216689, PMID: 22556251

Dong X, Shen K, Bülow HE. 2015. Intrinsic and extrinsic mechanisms of dendritic morphogenesis. *Annual Review of Physiology* **77**:271–300. DOI: https://doi.org/10.1146/annurev-physiol-021014-071746, PMID: 25386991

Droujinine IA, Perrimon N. 2016. Interorgan communication pathways in physiology: focus on *Drosophila*. *Annual Review of Genetics* **50**:539–570. DOI: https://doi.org/10.1146/annurev-genet-121415-122024, PMID: 27732790

Ekas LA, Baeg GH, Flaherty MS, Ayala-Camargo A, Bach EA. 2006. Jak/stat signaling promotes regional specification by negatively regulating wingless expression in *Drosophila*. *Development* **133**:4721–4729. DOI: https://doi.org/10.1242/dev.02675, PMID: 17079268

Endo M, Minami Y. 2018. Diverse roles for the ror-family receptor tyrosine kinases in neurons and glial cells during development and repair of the nervous system. *Developmental Dynamics* **247**:24–32. DOI: https://doi.org/10.1002/dvdy.24515, PMID: 28470690

Filosa A, Barker AJ, Dal Maschio M, Baier H. 2016. Feeding state modulates behavioral choice and processing of prey stimuli in the zebrafish tectum. *Neuron* **90**:596–608. DOI: https://doi.org/10.1016/j.neuron.2016.03.014, PMID: 27146269

Frenquelli M, Caridi N, Antonini E, Storti F, Viganò V, Gaviraghi M, Occhionorelli M, Bianchessi S, Bongiovanni L, Spinelli A, Marcatti M, Belloni D, Ferrero E, Karki S, Brambilla P, Martinelli-Boneschi F, Colla S, Ponzoni M, DePinho RA, Tonon G. 2020. The Wnt receptor Ror2 drives the interaction of multiple myeloma cells with the

microenvironment through Akt activation. *Leukemia* **34**:257–270. DOI: https://doi.org/10.1038/s41375-019-0486-9, PMID: 31148590

Georgieff MK, Brunette KE, Tran PV. 2015. Early life nutrition and neural plasticity. *Development and Psychopathology* **27**:411–423. DOI: https://doi.org/10.1017/S0954579415000061, PMID: 25997762

González A, Hall MN, Lin SC, Hardie DG. 2020. Ampk and TOR: the yin and yang of cellular nutrient sensing and growth control. *Cell Metabolism* **31**:472–492. DOI: https://doi.org/10.1016/j.cmet.2020.01.015, PMID: 32130880

Green J, Nusse R, van Amerongen R. 2014. The role of Ryk and ROR receptor tyrosine kinases in Wnt signal transduction. *Cold Spring Harbor Perspectives in Biology* **6**:a009175. DOI: https://doi.org/10.1101/cshperspect.a009175, PMID: 24370848

Grueber WB, Jan LY, Jan YN. 2002. Tiling of the *Drosophila* epidermis by multidendritic sensory neurons. *Development* **129**:2867–2878. DOI: https://doi.org/10.1242/dev.129.12.2867, PMID: 12050135

Grueber WB, Ye B, Yang CH, Younger S, Borden K, Jan LY, Jan YN. 2007. Projections of *Drosophila* multidendritic neurons in the central nervous system: links with peripheral dendrite morphology. *Development* **134**:55–64. DOI: https://doi.org/10.1242/dev.02666, PMID: 17164414

Guntur AR, Gu P, Takle K, Chen J, Xiang Y, Yang CH. 2015. *Drosophila* TRPA1 isoforms detect UV light via photochemical production of H_2O_2. *PNAS* **112**:E5753–E5761. DOI: https://doi.org/10.1073/pnas.1514862112

Han C, Jan LY, Jan YN. 2011. Enhancer-driven membrane markers for analysis of nonautonomous mechanisms reveal neuron-glia interactions in *Drosophila*. *PNAS* **108**:9673–9678. DOI: https://doi.org/10.1073/pnas.1106386108

Han C, Wang D, Soba P, Zhu S, Lin X, Jan LY, Jan YN. 2012. Integrins regulate repulsion-mediated dendritic patterning of *Drosophila* sensory neurons by restricting dendrites in a 2D space. *Neuron* **73**:64–78. DOI: https://doi.org/10.1016/j.neuron.2011.10.036, PMID: 22243747

Harris RE, Setiawan L, Saul J, Hariharan IK. 2016. Localized epigenetic silencing of a damage-activated WNT enhancer limits regeneration in mature *Drosophila* imaginal discs. *eLife* **5**:e11588. DOI: https://doi.org/10.7554/eLife.11588, PMID: 26840050

Hattori Y, Usui T, Satoh D, Moriyama S, Shimono K, Itoh T, Shirahige K, Uemura T. 2013. Sensory-neuron subtype-specific transcriptional programs controlling dendrite morphogenesis: genome-wide analysis of abrupt and knot/collier. *Developmental Cell* **27**:530–544. DOI: https://doi.org/10.1016/j.devcel.2013.10.024, PMID: 24290980

He CW, Liao CP, Pan CL. 2018. Wnt signalling in the development of axon, dendrites and synapses. *Open Biology* **8**:180116. DOI: https://doi.org/10.1098/rsob.180116, PMID: 30282660

Homem CCF, Repic M, Knoblich JA. 2015. Proliferation control in neural stem and progenitor cells. *Nature Reviews. Neuroscience* **16**:647–659. DOI: https://doi.org/10.1038/nrn4021, PMID: 26420377

Hoyer N, Zielke P, Hu C, Petersen M, Sauter K, Scharrenberg R, Peng Y, Kim CC, Han C, Parrish JZ, Soba P. 2018. Ret and substrate-derived TGF-β maverick regulate space-filling dendrite growth in *Drosophila* sensory neurons. *Cell Reports* **24**:2261–2272.. DOI: https://doi.org/10.1016/j.celrep.2018.07.092, PMID: 30157422

Hughes CL, Thomas JB. 2007. A sensory feedback circuit coordinates muscle activity in *Drosophila*. *Molecular and Cellular Neurosciences* **35**:383–396. DOI: https://doi.org/10.1016/j.mcn.2007.04.001, PMID: 17498969

Hwang RY, Zhong L, Xu Y, Johnson T, Zhang F, Deisseroth K, Tracey WD. 2007. Nociceptive neurons protect *Drosophila* larvae from parasitoid wasps. *Current Biology* **17**:2105–2116. DOI: https://doi.org/10.1016/j.cub.2007.11.029, PMID: 18060782

Im SH, Galko MJ. 2012. Pokes, sunburn, and hot sauce: *Drosophila* as an emerging model for the biology of nociception. *Developmental Dynamics* **241**:16–26. DOI: https://doi.org/10.1002/dvdy.22737, PMID: 21932321

Imambocus BN, Zhou F, Formozov A, Wittich A, Tenedini FM, Hu C, Sauter K, Macarenhas Varela E, Herédia F, Casimiro AP, Macedo A, Schlegel P, Yang C-H, Miguel-Aliaga I, Wiegert JS, Pankratz MJ, Gontijo AM, Cardona A, Soba P. 2022. A neuropeptidergic circuit gates selective escape behavior of *Drosophila* larvae. *Current Biology* **32**:149–163. DOI: https://doi.org/10.1016/j.cub.2021.10.069, PMID: 34798050

Jan YN, Jan LY. 2010. Branching out: mechanisms of dendritic arborization. *Nature Reviews. Neuroscience* **11**:316–328. DOI: https://doi.org/10.1038/nrn2836, PMID: 20404840

Jaszczak JS, DeVault L, Jan LY, Jan YN. 2022. Steroid hormone signaling activates thermal nociception during *Drosophila* peripheral nervous system development. *eLife* **11**:e76464. DOI: https://doi.org/10.7554/eLife.76464, PMID: 35353036

Jayakumar S, Richhariya S, Reddy OV, Texada MJ, Hasan G. 2016. *Drosophila* larval to pupal switch under nutrient stress requires IP3R/Ca (2+) signalling in glutamatergic interneurons. *eLife* **5**:e17495. DOI: https://doi.org/10.7554/eLife.17495, PMID: 27494275

Jayakumar S, Hasan G. 2018. Neuronal calcium signaling in metabolic regulation and adaptation to nutrient stress. *Frontiers in Neural Circuits* **12**:25. DOI: https://doi.org/10.3389/fncir.2018.00025, PMID: 29674958

Jayakumar S, Richhariya S, Deb BK, Hasan G. 2018. A multicomponent neuronal response encodes the larval decision to pupariate upon amino acid starvation. *The Journal of Neuroscience* **38**:10202–10219. DOI: https://doi.org/10.1523/JNEUROSCI.1163-18.2018, PMID: 30301757

Jiang N, Soba P, Parker E, Kim CC, Parrish JZ. 2014. The microrna bantam regulates a developmental transition in epithelial cells that restricts sensory dendrite growth. *Development* **141**:2657–2668. DOI: https://doi.org/10.1242/dev.107573, PMID: 24924190

Jiang N, Rasmussen JP, Clanton JA, Rosenberg MF, Luedke KP, Cronan MR, Parker ED, Kim HJ, Vaughan JC, Sagasti A, Parrish JZ. 2019. A conserved morphogenetic mechanism for epidermal ensheathment of nociceptive sensory neurites. *eLife* **8**:e42455. DOI: https://doi.org/10.7554/eLife.42455, PMID: 30855229

Kambe T, Nishito Y, Fukue K. 2016. Molecular, Genetic, and Nutritional Aspects of Major and Trace Minerals. Elsevier. DOI: https://doi.org/10.1016/C2014-0-02224-1

Kanaoka Y, Skibbe H, Hayashi Y, Uemura T, Hattori Y. 2019. DeTerm: software for automatic detection of neuronal dendritic branch terminals via an artificial neural network. *Genes to Cells* **24**:464–472. DOI: https://doi.org/10.1111/gtc.12700, PMID: 31095815

Kim ME, Shrestha BR, Blazeski R, Mason CA, Grueber WB. 2012. Integrins establish dendrite-substrate relationships that promote dendritic self-avoidance and patterning in *Drosophila* sensory neurons. *Neuron* **73**:79–91. DOI: https://doi.org/10.1016/j.neuron.2011.10.033, PMID: 22243748

Lee JH, Bassel-Duby R, Olson EN. 2014. Heart- and muscle-derived signaling system dependent on MED13 and wingless controls obesity in *Drosophila*. *PNAS* **111**:9491–9496. DOI: https://doi.org/10.1073/pnas.1409427111, PMID: 24979807

Lin W-Y, Williams C, Yan C, Koledachkina T, Luedke K, Dalton J, Bloomsburg S, Morrison N, Duncan KE, Kim CC, Parrish JZ. 2015. The SLC36 transporter pathetic is required for extreme dendrite growth in *Drosophila* sensory neurons. *Genes & Development* **29**:1120–1135. DOI: https://doi.org/10.1101/gad.259119.115, PMID: 26063572

Liu Y, Yang H, Chen T, Luo Y, Xu Z, Li Y, Yang J. 2015. Silencing of receptor tyrosine kinase Ror1 inhibits tumor-cell proliferation via PI3K/Akt/mTOR signaling pathway in lung adenocarcinoma. *PLOS ONE* **10**:e0127092. DOI: https://doi.org/10.1371/journal.pone.0127092, PMID: 25978653

Liu Q, Tabuchi M, Liu S, Kodama L, Horiuchi W, Daniels J, Chiu L, Baldoni D, Wu MN. 2017. Branch-Specific plasticity of a bifunctional dopamine circuit encodes protein hunger. Science **356**:534–539. DOI: https://doi.org/10.1126/science.aal3245, PMID: 28473588

Liu GY, Sabatini DM. 2020. Mtor at the nexus of nutrition, growth, ageing and disease. *Nature Reviews. Molecular Cell Biology* **21**:183–203. DOI: https://doi.org/10.1038/s41580-019-0199-y, PMID: 31937935

Matsubara D, Horiuchi SY, Shimono K, Usui T, Uemura T. 2011. The seven-pass transmembrane cadherin flamingo controls dendritic self-avoidance via its binding to a LIM domain protein, espinas, in *Drosophila* sensory neurons. *Genes & Development* **25**:1982–1996. DOI: https://doi.org/10.1101/gad.16531611, PMID: 21937715

McCarthy DJ, Chen Y, Smyth GK. 2012. Differential expression analysis of multifactor RNA-seq experiments with respect to biological variation. *Nucleic Acids Research* **40**:4288–4297. DOI: https://doi.org/10.1093/nar/gks042, PMID: 22287627

Meltzer S, Yadav S, Lee J, Soba P, Younger SH, Jin P, Zhang W, Parrish J, Jan LY, Jan YN. 2016. Epidermis-Derived semaphorin promotes dendrite self-avoidance by regulating dendrite-substrate adhesion in *Drosophila* sensory neurons. *Neuron* **89**:741–755. DOI: https://doi.org/10.1016/j.neuron.2016.01.020, PMID: 26853303

Meltzer S, Bagley JA, Perez GL, O'Brien CE, DeVault L, Guo Y, Jan LY, Jan Y-N. 2017. Phospholipid homeostasis regulates dendrite morphogenesis in *Drosophila* sensory neurons. *Cell Reports* **21**:859–866. DOI: https://doi.org/10.1016/j.celrep.2017.09.089, PMID: 29069593

Morton GJ, Meek TH, Schwartz MW. 2014. Neurobiology of food intake in health and disease. *Nature Reviews. Neuroscience* **15**:367–378. DOI: https://doi.org/10.1038/nrn3745, PMID: 24840801

Musselman LP, Fink JL, Narzinski K, Ramachandran PV, Hathiramani SS, Cagan RL, Baranski TJ. 2011. A high-sugar diet produces obesity and insulin resistance in wild-type *Drosophila*. *Disease Models & Mechanisms* **4**:842–849. DOI: https://doi.org/10.1242/dmm.007948, PMID: 21719444

Nye DMR, Albertson RM, Weiner AT, Hertzler JI, Shorey M, Goberdhan DCI, Wilson C, Janes KA, Rolls MM. 2020. The receptor tyrosine kinase ROR is required for dendrite regeneration in *Drosophila* neurons. *PLOS Biology* **18**:e3000657. DOI: https://doi.org/10.1371/journal.pbio.3000657, PMID: 32163406

Okamoto N, Nishimura T. 2015. Signaling from glia and cholinergic neurons controls nutrient-dependent production of an insulin-like peptide for *Drosophila* body growth. *Developmental Cell* **35**:295–310. DOI: https://doi.org/10.1016/j.devcel.2015.10.003, PMID: 26555050

Onodera K, Baba S, Murakami A, Uemura T, Usui T. 2017. Small conductance ca^{2+}-activated K^+ channels induce the firing pause periods during the activation of *Drosophila* nociceptive neurons. *eLife* **6**:e1. DOI: https://doi.org/10.7554/eLife.29754.001

Padilla SL, Qiu J, Soden ME, Sanz E, Nestor CC, Barker FD, Quintana A, Zweifel LS, Rønnekleiv OK, Kelly MJ, Palmiter RD. 2016. Agouti-Related peptide neural circuits mediate adaptive behaviors in the starved state. *Nature Neuroscience* **19**:734–741. DOI: https://doi.org/10.1038/nn.4274, PMID: 27019015

Parrish JZ, Xu P, Kim CC, Jan LY, Jan YN. 2009. The microRNA bantam functions in epithelial cells to regulate scaling growth of dendrite arbors in *Drosophila* sensory neurons. *Neuron* **63**:788–802. DOI: https://doi.org/10.1016/j.neuron.2009.08.006, PMID: 19778508

Piper MDW, Blanc E, Leitão-Gonçalves R, Yang M, He X, Linford NJ, Hoddinott MP, Hopfen C, Soultoukis GA, Niemeyer C, Kerr F, Pletcher SD, Ribeiro C, Partridge L. 2014. A holidic medium for *Drosophila melanogaster*. *Nature Methods* **11**:100–105. DOI: https://doi.org/10.1038/nmeth.2731, PMID: 24240321

Piper MDW, Soultoukis GA, Blanc E, Mesaros A, Herbert SL, Juricic P, He X, Atanassov I, Salmonowicz H, Yang M, Simpson SJ, Ribeiro C, Partridge L. 2017. Matching dietary amino acid balance to the in silico-translated exome optimizes growth and reproduction without cost to lifespan. *Cell Metabolism* **25**:610–621. DOI: https://doi.org/10.1016/j.cmet.2017.02.005, PMID: 28273481

Poe AR, Tang L, Wang B, Li Y, Sapar ML, Han C. 2017. Dendritic space-filling requires a neuronal type-specific extracellular permissive signal in *Drosophila*. *PNAS* **114**:E8062–E8071. DOI: https://doi.org/10.1073/pnas.1707467114, PMID: 28874572

Poe AR, Xu Y, Zhang C, Lei J, Li K, Labib D, Han C. 2020. Low foxo expression in *Drosophila* somatosensory neurons protects dendrite growth under nutrient restriction. *eLife* **9**:47. DOI: https://doi.org/10.7554/eLife.53351, PMID: 32427101

Prado EL, Dewey KG. 2014. Nutrition and brain development in early life. *Nutrition Reviews* **72**:267–284. DOI: https://doi.org/10.1111/nure.12102, PMID: 24684384

Rajan A, Perrimon N. 2012. *Drosophila* cytokine unpaired 2 regulates physiological homeostasis by remotely controlling insulin secretion. *Cell* **151**:123–137. DOI: https://doi.org/10.1016/j.cell.2012.08.019, PMID: 23021220

Ripp C, Loth J, Petrova I, Linnemannstöns K, Ulepic M, Fradkin L, Noordermeer J, Wodarz A. 2018. *Drosophila* ROR is a nervous system-specific co-receptor for Wnt ligands. *Biology Open* **7**:bio033001. DOI: https://doi.org/10.1242/bio.033001, PMID: 30341100

Robinson MD, McCarthy DJ, Smyth GK. 2010. EdgeR: a bioconductor package for differential expression analysis of digital gene expression data. *Bioinformatics* **26**:139–140. DOI: https://doi.org/10.1093/bioinformatics/btp616, PMID: 19910308

Schuster CM, Davis GW. 1996. Genetic dissection of structural and functional components of synaptic plasticity. I. fasciclin II controls synaptic stabilization and growth. *Neuron* **1**:641–654. DOI: https://doi.org/10.1016/S0896-6273(00)80197-X, PMID: 8893022

Shim J, Gururaja-Rao S, Banerjee U. 2013. Nutritional regulation of stem and progenitor cells in *Drosophila*. *Development* **140**:4647–4656. DOI: https://doi.org/10.1242/dev.079087, PMID: 24255094

Shimada-Niwa Y, Niwa R. 2014. Serotonergic neurons respond to nutrients and regulate the timing of steroid hormone biosynthesis in *Drosophila*. *Nature Communications* **5**:5778. DOI: https://doi.org/10.1038/ncomms6778, PMID: 25502946

Shimono K, Fujishima K, Nomura T, Ohashi M, Usui T, Kengaku M, Toyoda A, Uemura T. 2014. An evolutionarily conserved protein chord regulates scaling of dendritic arbors with body size. *Scientific Reports* **4**:4415. DOI: https://doi.org/10.1038/srep04415, PMID: 24643112

Sopko R, Perrimon N. 2013. Receptor tyrosine kinases in *Drosophila* development. *Cold Spring Harbor Perspectives in Biology* **5**:a009050. DOI: https://doi.org/10.1101/cshperspect.a009050, PMID: 23732470

Stocker H, Andjelkovic M, Oldham S, Laffargue M, Wymann MP, Hemmings BA, Hafen E. 2002. Living with lethal PIP3 levels: viability of flies lacking PTEN restored by a PH domain mutation in akt/PKB. *Science* **295**:2088–2091. DOI: https://doi.org/10.1126/science.1068094

St Pierre SE, Galindo MI, Couso JP, Thor S. 2002. Control of *Drosophila* imaginal disc development by rotund and roughened eye: differentially expressed transcripts of the same gene encoding functionally distinct zinc finger proteins. *Development* **129**:1273–1281. DOI: https://doi.org/10.1242/dev.129.5.1273, PMID: 11874922

Symmonds M, Emmanuel JJ, Drew ME, Batterham RL, Dolan RJ. 2010. Metabolic state alters economic decision making under risk in humans. *PLOS ONE* **5**:e11090. DOI: https://doi.org/10.1371/journal.pone.0011090, PMID: 20585383

Tenenbaum CM, Misra M, Alizzi RA, Gavis ER. 2017. Enclosure of dendrites by epidermal cells restricts branching and permits coordinated development of spatially overlapping sensory neurons. *Cell Reports* **20**:3043–3056. DOI: https://doi.org/10.1016/j.celrep.2017.09.001, PMID: 28954223

Terada SI, Matsubara D, Onodera K, Matsuzaki M, Uemura T, Usui T. 2016. Neuronal processing of noxious thermal stimuli mediated by dendritic ca(2+) influx in *Drosophila* somatosensory neurons. *eLife* **5**:e12959. DOI: https://doi.org/10.7554/eLife.12959, PMID: 26880554

Texada MJ, Koyama T, Rewitz K. 2020. Regulation of body size and growth control. *Genetics* **216**:269–313. DOI: https://doi.org/10.1534/genetics.120.303095, PMID: 33023929

Tracey WD, Wilson RI, Laurent G, Benzer S. 2003. Painless, a *Drosophila* gene essential for nociception. *Cell* **113**:261–273. DOI: https://doi.org/10.1016/s0092-8674(03)00272-1, PMID: 12705873

Tsubouchi A, Caldwell JC, Tracey WD. 2012. Dendritic filopodia, ripped pocket, NOMPC, and nmdars contribute to the sense of touch in *Drosophila* larvae. *Current Biology* **22**:2124–2134. DOI: https://doi.org/10.1016/j.cub.2012.09.019, PMID: 23103192

Valnegri P, Puram SV, Bonni A. 2015. Regulation of dendrite morphogenesis by extrinsic cues. *Trends in Neurosciences* **38**:439–447. DOI: https://doi.org/10.1016/j.tins.2015.05.003, PMID: 26100142

van Amerongen R, Nusse R. 2009. Towards an integrated view of wnt signaling in development. *Development* **136**:3205–3214. DOI: https://doi.org/10.1242/dev.033910, PMID: 19736321

Watanabe K, Furumizo Y, Usui T, Hattori Y, Uemura T. 2017. Nutrient-dependent increased dendritic arborization of somatosensory neurons. *Genes to Cells* **22**:105–114. DOI: https://doi.org/10.1111/gtc.12451, PMID: 27868313

Watanabe K, Kanaoka Y, Mizutani S, Uchiyama H, Yajima S, Watada M, Uemura T, Hattori Y. 2019. Interspecies comparative analyses reveal distinct carbohydrate-responsive systems among *Drosophila* species. *Cell Reports* **28**:2594–2607. DOI: https://doi.org/10.1016/j.celrep.2019.08.030

Weiner AT, Seebold DY, Torres-Gutierrez P, Folker C, Swope RD, Kothe,GO, Stoltz JG, Zalenski MK, Kozlowski C, Barbera DJ. 2020. Endosomal wnt signaling proteins control microtubule nucleation in dendrites. *PLOS Biology* **18**:647. DOI: https://doi.org/10.1371/journal.pbio.3000647

Xiang Y, Yuan Q, Vogt N, Looger LL, Jan LY, Jan YN. 2010. Light-avoidance-mediating photoreceptors tile the *Drosophila* larval body wall. *Nature* **468**:921–926. DOI: https://doi.org/10.1038/nature09576, PMID: 21068723

Yamanaka N, Romero NM, Martin FA, Rewitz KF, Sun M, O'Connor MB, Léopold P. 2013. Neuroendocrine control of *Drosophila* larval light preference. *Science* **341**:1113–1116. DOI: https://doi.org/10.1126/science.1241210

Yan Z, Zhang W, He Y, Gorczyca D, Xiang Y, Cheng LE, Meltzer S, Jan LY, Jan YN. 2013. *Drosophila* NOMPC is a mechanotransduction channel subunit for gentle-touch sensation. *Nature* **493**:221–225. DOI: https://doi.org/10.1038/nature11685, PMID: 23222543

Yang H, Kronhamn J, Ekström J-O, Korkut GG, Hultmark D. 2015. Jak/Stat signaling in *Drosophila* muscles controls the cellular immune response against parasitoid infection. *EMBO Reports* **16**:1664–1672. DOI: https://doi.org/10.15252/embr.201540277, PMID: 26412855

Yang WK, Chien CT. 2019. Beyond being innervated: the epidermis actively shapes sensory dendritic patterning. *Open Biology* **9**:180257. DOI: https://doi.org/10.1098/rsob.180257, PMID: 30914004

Yasunaga K, Kanamori T, Morikawa R, Suzuki E, Emoto K. 2010. Dendrite reshaping of adult *Drosophila* sensory neurons requires matrix metalloproteinase-mediated modification of the basement membranes. *Developmental Cell* **18**:621–632. DOI: https://doi.org/10.1016/j.devcel.2010.02.010, PMID: 20412776

Zhong L, Hwang RY, Tracey WD. 2010. Pickpocket is a DEG/ENaC protein required for mechanical nociception in *Drosophila* larvae. *Current Biology* **20**:429–434. DOI: https://doi.org/10.1016/j.cub.2009.12.057, PMID: 20171104

Ziegler AB, Thiele C, Tenedini F, Richard M, Leyendecker P, Hoermann A, Soba P, Tavosanis G. 2017. Cell-Autonomous control of neuronal dendrite expansion via the fatty acid synthesis regulator SREBP. *Cell Reports* **21**:3346–3353. DOI: https://doi.org/10.1016/j.celrep.2017.11.069, PMID: 29262315

Appendix 1

Appendix 1—key resources table

Reagent type (species) or resource	Designation	Source or reference	Identifiers	Additional information
genetic reagent (*Drosophila melanogaster*)	*ppk-GAL4 UAS-mCD8:GFP*	***Grueber et al., 2007*** (https://doi.org/10.1242/dev.02666)	N/A	
genetic reagent (*D. melanogaster*)	*Gr28b.c-GAL4 UAS-mCD8:GFP*	***Xiang et al., 2010*** (https://doi.org/10.1038/nature09576)	N/A	
genetic reagent (*D. melanogaster*)	*ppk-CD4-tdGFP^{1b}*	***Han et al., 2011*** (https://doi.org/10.1073/pnas.1106386108)	N/A	
genetic reagent (*D. melanogaster*)	*ppk-CD4-tdGFP^{8}*	***Han et al., 2011*** (https://doi.org/10.1073/pnas.1106386108)	N/A	
genetic reagent (*D. melanogaster*)	*ppk-CD4-tdTom^{4a}*	***Han et al., 2011*** (https://doi.org/10.1073/pnas.1106386108)	N/A	
genetic reagent (*D. melanogaster*)	*Ror^{4}*	***Ripp et al., 2018*** (https://doi.org/10.1242/bio.033001)	N/A	
genetic reagent (*D. melanogaster*)	*ppk-GAL4*	Bloomington *Drosophila* Stock Center	Stock #: 32079	
genetic reagent (*D. melanogaster*)	*Mhc-GAL4*	***Schuster and Davis, 1996*** (https://doi.org/10.1016/s0896-6273(00)80,197x)	N/A	
genetic reagent (*D. melanogaster*)	*Cg-GAL4*	Bloomington *Drosophila* Stock Center	Stock #: 7011	
genetic reagent (*D. melanogaster*)	*ap^{ts78j} wg^{1}*	KYOTO Stock Center	Stock #: 107069	
genetic reagent (*D. melanogaster*)	*wg^{l-8} cn^{1} bw^{1} speck^{1}*	KYOTO Stock Center	Stock #: 107019	
genetic reagent (*D. melanogaster*)	*wg-GAL4*	Bloomington *Drosophila* Stock Center	Stock #: 83627	
genetic reagent (*D. melanogaster*)	*UAS-RedStinger*	Bloomington *Drosophila* Stock Center	Stock #: 8547	
genetic reagent (*D. melanogaster*)	*UAS-Akt RNAi* (BL33615)	Bloomington *Drosophila* Stock Center	Stock #: 33615	
genetic reagent (*D. melanogaster*)	*UAS-Akt RNAi* (v2902)	Vienna *Drosophila* Resource Center	Stock #: 2902	
genetic reagent (*D. melanogaster*)	*UAS-Ror RNAi*	National Institute of Genetics	Stock #: 4926 R-1	
genetic reagent (*D. melanogaster*)	*UAS-wg RNAi*	Vienna *Drosophila* Resource Center	Stock #: 6692	
genetic reagent (*D. melanogaster*)	*UAS-Stat92E RNAi* (BL33637)	Bloomington *Drosophila* Stock Center	Stock #: 33637	
genetic reagent (*D. melanogaster*)	*UAS-hop RNAi*	Bloomington *Drosophila* Stock Center	Stock #: 32966	
genetic reagent (*D. melanogaster*)	*UAS-upd2 RNAi* (5988 R-1)	National Institute of Genetics	Stock #: 5988 R-1	
genetic reagent (*D. melanogaster*)	*UAS-hop*	Bloomington *Drosophila* Stock Center	Stock #: 79033	
genetic reagent (*D. melanogaster*)	*UAS-myrAkt*	Bloomington *Drosophila* Stock Center	Stock #: 50758	
genetic reagent (*D. melanogaster*)	*UAS-wg.H.T:HA1*	KYOTO Stock Center	Stock #: 108488	
genetic reagent (*D. melanogaster*)	*10XSTAT92E-GFP*	Bloomington *Drosophila* Stock Center	Stock #: 26197	
genetic reagent (*D. melanogaster*)	*UAS-InR RNAi* (BL31594)	Bloomington *Drosophila* Stock Center	Stock #: 31594	
genetic reagent (*D. melanogaster*)	*UAS-InR RNAi* (BL51518)	Bloomington *Drosophila* Stock Center	Stock #: 51518	

Appendix 1 Continued on next page

Appendix 1 Continued

Reagent type (species) or resource	Designation	Source or reference	Identifiers	Additional information
genetic reagent (*D. melanogaster*)	*UAS-grnd RNAi*	Vienna *Drosophila* Resource Center	Stock #: 43454	
genetic reagent (*D. melanogaster*)	*UAS-wgn RNAi*	Vienna *Drosophila* Resource Center	Stock #: 9152	
genetic reagent (*D. melanogaster*)	*UAS-mth RNAi*	Vienna *Drosophila* Resource Center	Stock #: 102303	
genetic reagent (*D. melanogaster*)	*UAS-babo RNAi*	Bloomington *Drosophila* Stock Center	Stock #: 25933	
genetic reagent (*D. melanogaster*)	*UAS-Tor.TED*	Bloomington *Drosophila* Stock Center	Stock #: 7013	
genetic reagent (*D. melanogaster*)	*UAS-S6k.KQ*	Bloomington *Drosophila* Stock Center	Stock #: 6911	
genetic reagent (*D. melanogaster*)	*UAS-Tif-IA RNAi*	Vienna *Drosophila* Resource Center	Stock #: 20336	
genetic reagent (*D. melanogaster*)	*UAS-Thor RNAi*	Vienna *Drosophila* Resource Center	Stock #: 35439	
genetic reagent (*D. melanogaster*)	*UAS-foxo RNAi*	Bloomington *Drosophila* Stock Center	Stock #: 32427	
genetic reagent (*D. melanogaster*)	*UAS-Alk RNAi* (v11446)	Vienna *Drosophila* Resource Center	Stock #: 11446	
genetic reagent (*D. melanogaster*)	*UAS-Alk RNAi* (BL107083)	Vienna *Drosophila* Resource Center	Stock #: 107083	
genetic reagent (*D. melanogaster*)	*mef2-GAL4*	Bloomington *Drosophila* Stock Center	Stock #: 27390	
genetic reagent (*D. melanogaster*)	*R38F11-GAL4*	Bloomington *Drosophila* Stock Center	Stock #: 50014	
genetic reagent (*D. melanogaster*)	*UAS-fz RNAi*	Vienna *Drosophila* Resource Center	Stock #: 43075	
genetic reagent (*D. melanogaster*)	*UAS-fz2 RNAi*	National Institute of Genetics	Stock #: 9739 R-1	
genetic reagent (*D. melanogaster*)	*"GAL4$^{5\text{-}40}$ UAS-Venus:pm SOP-FLP#42; tubPGal80 FRT2A"*	KYOTO Stock Center	Stock #: 109950	
genetic reagent (*D. melanogaster*)	*"w*; FRT2A"*	KYOTO Stock Center	Stock #: 106623	
genetic reagent (*D. melanogaster*)	*"y w hs-flp; fz2^{C2} FRT2A"*	**Chen and Struhl, 1999** (https://doi.org/10.1242/dev.126.23.5441)	N/A	
genetic reagent (*D. melanogaster*)	*UAS-dsh RNAi*	Vienna *Drosophila* Resource Center	Stock #: 101525	
genetic reagent (*D. melanogaster*)	*UAS-bsk.DN*	Bloomington *Drosophila* Stock Center	Stock #: 6409	
genetic reagent (*D. melanogaster*)	*UAS-DAAM RNAi*	Vienna *Drosophila* Resource Center	Stock #: 24885	
genetic reagent (*D. melanogaster*)	*UAS-arm RNAi*	Vienna *Drosophila* Resource Center	Stock #: 7767	
genetic reagent (*D. melanogaster*)	*UAS-norpA RNAi*	Bloomington *Drosophila* Stock Center	Stock #: 31113	
genetic reagent (*D. melanogaster*)	*UAS-Axn RNAi*	Bloomington *Drosophila* Stock Center	Stock #: 31703	
genetic reagent (*D. melanogaster*)	*UAS-Stat92E RNAi* (BL31318)	Bloomington *Drosophila* Stock Center	Stock #: 31318	
genetic reagent (*D. melanogaster*)	*UAS-dome RNAi* (v106071)	Vienna *Drosophila* Resource Center	Stock #: 106071	
genetic reagent (*D. melanogaster*)	*UAS-dome RNAi* (BL32860)	Bloomington *Drosophila* Stock Center	Stock #: 32860	

Appendix 1 Continued on next page

Appendix 1 Continued

Reagent type (species) or resource	Designation	Source or reference	Identifiers	Additional information
genetic reagent (*D. melanogaster*)	*UAS-dome RNAi* (BL34618)	Bloomington *Drosophila* Stock Center	Stock #: 34618	
genetic reagent (*D. melanogaster*)	*UAS-upd RNAi* (BL33680)	Bloomington *Drosophila* Stock Center	Stock #: 33680	
genetic reagent (*D. melanogaster*)	*UAS-upd RNAi* (v3282)	Vienna *Drosophila* Resource Center	Stock #: 3282	
genetic reagent (*D. melanogaster*)	*UAS-upd2 RNAi* (BL33949)	Bloomington *Drosophila* Stock Center	Stock #: 33949	
genetic reagent (*D. melanogaster*)	*UAS-upd3 RNAi* (BL32859)	Bloomington *Drosophila* Stock Center	Stock #: 32859	
genetic reagent (*D. melanogaster*)	*UAS-upd3 RNAi* (BL28575)	Bloomington *Drosophila* Stock Center	Stock #: 28575	
genetic reagent (*D. melanogaster*)	*rn-GAL4*	***St Pierre et al., 2002*** (https://doi.org/10.1242/dev.129.5.1273)	N/A	
genetic reagent (*D. melanogaster*)	*UAS-dilp8*	***Colombani et al., 2012*** (https://doi.org/10.1126/science.1216689)	N/A	
genetic reagent (*D. melanogaster*)	*UAS-htl RNAi* (v6692)	Vienna *Drosophila* Resource Center	Stock #: 6692	
genetic reagent (*D. melanogaster*)	*UAS-htl RNAi* (BL35024)	Bloomington *Drosophila* Stock Center	Stock #: 35024	
genetic reagent (*D. melanogaster*)	*UAS-Egfr RNAi*	Vienna *Drosophila* Resource Center	Stock #: 43267	
genetic reagent (*D. melanogaster*)	*UAS-Pvr RNAi*	Vienna *Drosophila* Resource Center	Stock #: 13502	
genetic reagent (*D. melanogaster*)	*UAS-Ddr RNAi*	Vienna *Drosophila* Resource Center	Stock #: 29720	
genetic reagent (*D. melanogaster*)	*UAS-dnt RNAi*	National Institute of Genetics	Stock #: 17,559 R-3	
genetic reagent (*D. melanogaster*)	*UAS-drl RNAi*	Bloomington *Drosophila* Stock Center	Stock #: 29602	
genetic reagent (*D. melanogaster*)	*UAS-Eph RNAi*	Bloomington *Drosophila* Stock Center	Stock #: 28511	
genetic reagent (*D. melanogaster*)	*UAS-otk RNAi*	Bloomington *Drosophila* Stock Center	Stock #: 25790	
genetic reagent (*D. melanogaster*)	*UAS-sev RNAi*	Bloomington *Drosophila* Stock Center	Stock #: 31274	
genetic reagent (*D. melanogaster*)	*UAS-btl RNAi*	Vienna *Drosophila* Resource Center	Stock #: 110277	
genetic reagent (*D. melanogaster*)	*UAS-Cad96Ca RNAi*	Vienna *Drosophila* Resource Center	Stock #: 1089	
genetic reagent (*D. melanogaster*)	*UAS-CG10702 RNAi*	Vienna *Drosophila* Resource Center	Stock #: 27052	
genetic reagent (*D. melanogaster*)	*UAS-Drl-2 RNAi*	Vienna *Drosophila* Resource Center	Stock #: 40484	
genetic reagent (*D. melanogaster*)	*UAS-Nrk RNAi*	Vienna *Drosophila* Resource Center	Stock #: 9653	
genetic reagent (*D. melanogaster*)	*UAS-Ret RNAi*	Vienna *Drosophila* Resource Center	Stock #: 107648	
genetic reagent (*D. melanogaster*)	*UAS-tor RNAi*	Vienna *Drosophila* Resource Center	Stock #: 36280	
genetic reagent (*D. melanogaster*)	*UAS-Tie RNAi*	Vienna *Drosophila* Resource Center	Stock #: 26879	
genetic reagent (*D. melanogaster*)	$Gal4^{19\text{-}12}$	***Xiang et al., 2010*** (https://doi.org/10.1038/nature09576)	N/A	
antibody	anti-Wg (Mouse monoclonal)	Developmental Studies Hybridoma Bank	Cat# 4D4, RRID: AB_528512	IF (1:15)

Appendix 1 Continued on next page

Appendix 1 Continued

Reagent type (species) or resource	Designation	Source or reference	Identifiers	Additional information
antibody	anti-Futch (Mouse monoclonal)	Developmental Studies Hybridoma Bank	Cat# 22C10, RRID: AB_528403	IF (1:20)
antibody	anti-phospho-Akt (Rabbit polyclonal)	Cell Signaling	Cat# 9271 S	IF (1:100)
antibody	anti-DsRed (Rabbit polyclonal)	Clontech	Cat# 632496	IF (1:250)
antibody	anti-Mouse IgG Alexa Fluor 488 (Goat polyclonal)	Invitrogen	Cat# A11029	IF (1:1000)
antibody	anti-Rabbit IgG Alexa Fluor 488 (Goat polyclonal)	Invitrogen	Cat# A11034	IF (1:1000)
antibody	anti-Mouse IgG Alexa Fluor 546 (Goat polyclonal)	Invitrogen	Cat# A11030	IF (1:1000)
chemical compound, drug	Brewer's Yeast	MPBio	Cat# 2903312	
chemical compound, drug	Yeast extract	Sigma-Aldrich Fluka	Cat# 70161	
chemical compound, drug	Peptone from casein, enzymatic digest	Sigma-Aldrich Fluka	Cat# 82303	
chemical compound, drug	Glucose	Wako	Cat# 049–31165	
chemical compound, drug	Sucrose	Wako	Cat# 196–00015	
chemical compound, drug	$MgSO_4$	Wako	Cat# 132–00435	
chemical compound, drug	$CaCl_2$	Wako	Cat# 031–00435	
chemical compound, drug	agar	Matsuki Kanten	N/A	
chemical compound, drug	Agar Purified, powder	Nacalai Tesque	Cat# 01162–15	
chemical compound, drug	propionic acid	Nacalai Tesque	Cat# 29018–55	
chemical compound, drug	butyl p-hydroxybenzoate	Nacalai Tesque	Cat# 06327–02	
chemical compound, drug	50 x MEM Essential Amino Acids Solution	Wako	Cat# 132–15641	
chemical compound, drug	BSA	Nacalai Tesque	Cat# 01863–77	
chemical compound, drug	Alexa Fluor 488 Phalloidin	Invitrogen	Cat# A12379	
chemical compound, drug	FluorSave Reagent	Calbiochem	Cat# 345789	
chemical compound, drug	Formalin	Nacalai Tesque	Cat# 16222–65	
chemical compound, drug	DAPI	Nacalai Tesque	Cat# 19178–91	
software, algorithm	DeTerm	***Kanaoka et al., 2019*** (https://doi.org/10.1111/gtc.12700)	N/A	
software, algorithm	R	R Core Team	RRID:SCR_001905	
software, algorithm	Fiji	NIH	RRID:SCR_002285	
software, algorithm	Photoshop	Adobe	RRID:SCR_014199	
other	LED desk light	OHM	Cat# ODS-LKL6-W	This LED light was used in Light/dark choice assay